

SPIN AND MAGNETISM OF WHITE DWARFS

YEVGENI KISSIN

Department of Astronomy and Astrophysics, University of Toronto, 50 St. George St., Toronto, ON M5S 3H4, Canada

CHRISTOPHER THOMPSON

Canadian Institute for Theoretical Astrophysics, 60 St. George St., Toronto, ON M5H 3H8, Canada

Draft version July 12, 2021

ABSTRACT

The magnetism and rotation of white dwarf (WD) stars are investigated in relation to a hydromagnetic dynamo operating in the progenitor during shell burning phases. The downward pumping of angular momentum in the convective envelope, in combination with the absorption of a planet or tidal spin-up from a binary companion, can trigger strong dynamo action near the core-envelope boundary. Several arguments point to the outer core as the source for a magnetic field in the WD remnant: the outer third of a $\sim 0.55 M_{\odot}$ WD is processed during the shell burning phase(s) of the progenitor; the escape of magnetic helicity through the envelope mediates the growth of (compensating) helicity in the core, as is needed to maintain a stable magnetic field in the remnant; and the intense radiation flux at the core boundary facilitates magnetic buoyancy within a relatively thick tachocline layer. The helicity flux into the growing core is driven by a dynamical imbalance with a latitude-dependent rotational stress. The magnetic field deposited in an isolated massive WD is concentrated in an outer shell of mass $\lesssim 0.1 M_{\odot}$ and can reach ~ 10 MG. A buried toroidal field experiences moderate ohmic decay above an age ~ 0.3 Gyr, which may lead to growth or decay of the external magnetic field. The final WD spin period is related to a critical spin rate below which magnetic activity shuts off, and core and envelope decouple; it generally sits in the range of hours to days. WD periods ranging up to a year are possible if the envelope re-expands following a late thermal pulse.

Subject headings: stars: giants – stars: white dwarfs – stars: rotation – magnetic fields

1. INTRODUCTION

The magnetic field and spin of a white dwarf (WD) are inherited from its progenitor star. Our interest here is in how magnetism and rotation evolve together within the progenitor, in response to an active hydromagnetic dynamo. We focus on the post-main sequence phase of stellar evolution, when the material comprising the outer layers of the WD is deposited by a strong inflow from a hydrogen-rich convective envelope, through burning shell(s), into the stellar core. The presence or absence of a magnetic field at the surface of the WD remnant depends on the ability of the inner envelope to sustain a magnetic field.

Rotationally-driven dynamo activity on the red giant (RGB) and asymptotic giant (AGB) branch has received only limited attention (e.g. Blackman et al. 2001; Nordhaus et al. 2008), due to a prevailing assumption that the radial angular velocity profile $\Omega(r)$ in the convective envelope will mirror that observed in the Sun. Although localized magnetic field amplification in the outer, slowly rotating envelope may result in weak surface magnetic fields (Dorch 2004; Aurière et al. 2010), a dynamo that manifests itself through strong chromospheric and coronal emission appears to depend on an interaction with a binary stellar companion, as in RSCvn stars (e.g. Moss et al. 1991). Magnetic activity appears to be prevalent during the first stages of post-MS expansion, and during core helium burning (Aurière et al. 2014), but the sampling of more expanded giants is very limited.

On the other hand, the angular velocity profile in a

giant is less sensitive to boundary conditions than it is in the Sun, given the extreme depth of the envelope. Here we are guided by i) recent measurements of rapid core rotation in subgiants and core He burning stars using asteroseismic measurements by Kepler (Beck et al. 2012; Mosser et al. 2012); ii) measurements of a strong decrease of surface rotation speeds in subgiants as they evolve toward the RGB (Schrijver & Pols 1993); and iii) anelastic simulations which show a tendency to nearly uniform specific angular momentum in a deep convective envelope with slow rotation (Brun & Palacios 2009).

In a companion paper (Kissin & Thompson 2015, hereafter paper I), we show that the Kepler measurements are consistent with a tight coupling between the radiative core and convective envelope, combined with some inward pumping of angular momentum deep into the envelope. The favored rotation profile has $\Omega(r)$ transitioning between $\propto r^{-1}$ in the inner envelope to $\propto r^{-2}$ in the outer and more slowly rotating layers. The depth of the transition point depends on the size of the star and its angular momentum.

An important consequence of such an inward-peaked rotation profile is that the threshold for a rotationally driven dynamo may be reached in the inner envelope, but *not* near the stellar photosphere. A key figure of merit is the Coriolis parameter

$$\text{Co} \equiv \Omega \tau_{\text{con}} \equiv \frac{\Omega \ell_P}{v_{\text{con}}} \quad (1)$$

as measured at the base of the envelope; here v_{con} is the convective velocity and τ_{con} is the timescale for con-

vection over one pressure scale height. Observations of MS stars indicate the presence of dynamo activity when $\text{Co} \gtrsim 1$ (corresponding to a Rossby number $\lesssim 2\pi$; e.g. Reiners et al. 2009). The radial transition in the slope of the rotation profile in a deep convective envelope is postulated to occur where Co approaches unity, with the most rapidly rotating zone lying below this transition.

Inward pumping of angular momentum can also reduce the need for magnetically driven spindown in subgiants (Paper I).

1.1. *Remnant Magnetism: Dependence on Stellar Mass, Binarity and Age*

Three hypotheses have dominated previous discussions of the origin of magnetic fields in WD stars: the conservation of magnetic flux from the main sequence (MS) progenitor (Angel et al. 1981; Ferrario & Wickramasinghe 2005); the amplification of such a seed field by convective episodes in the core of the progenitor star (Ruderman & Sutherland 1973); and the transient amplification of the field during a merger event (Tout et al. 2008; Nordhaus et al. 2011).

We begin our investigation by reviewing some constraints on each of these hypotheses; and then summarize the arguments pointing to an amplification of the magnetic field during the post-MS expansion of the WD progenitor. This process comprises three steps: i) the advection of angular momentum inward through the convective envelope; ii) the amplification of a magnetic field by a dynamo near the core-envelope boundary; followed by iii) a flow of magnetic helicity into the growing core, which is sustained by a persistent angular velocity gradient and magnetic twist below the boundary.

Whether the inner envelope can support a dynamo turns out to depend on a combination of stellar properties. The core rotation rate is sensitive to the loss of angular momentum on the MS, and to any interaction with a planetary or stellar companion. Clearly solid rotation would imply $\text{Co} \ll 1$ throughout the envelope of a star approaching the tip of the RGB or AGB; and therefore suggest the absence of a large-scale hydromagnetic dynamo. But when the envelope rotation profile is inwardly peaked, we find differing answers for isolated stars of initial mass M_{ZAMS} less or greater than $\sim 1.3 M_{\odot}$, corresponding to the presence or absence of a strong magnetic wind on the MS. Hence the greater importance of binary interaction for sustaining $\text{Co} \gtrsim 1$ in solar-mass stars.

Another consideration is the proportion of the material contained in the remnant WD that is deposited during single and double shell burning. This comprises about a third of the mass of the WD when $M_{\text{ZAMS}} \sim 1$ ($M_{\text{wd}} \sim 0.55 M_{\odot}$), but is strongly reduced by dredge-up (after core helium ignition and before the onset of thermal pulses) in the intermediate-mass stars that are the progenitors of massive WDs. In this second case, the magnetized mass shell turns out to be thin enough that ohmic decay is initiated on a timescale ~ 0.3 Gyr (with some dependence on the mass loss rate on the AGB).

The source of a strong magnetic field ($1 - 10^3$ MG) in a WD therefore depends on both its age and mass. Indeed, expanded sampling of WD magnetism calls into question the flux-freezing hypothesis. Whereas between ~ 2 and ~ 10 percent of isolated WDs are magnetic in

this sense (Liebert et al. 2003, 2005) – roughly similar to the proportion of chemically peculiar and magnetic A stars – the proportion is higher in isolated massive WDs (Kepler et al. 2013) and extends to ~ 25 percent in cataclysmic variables (CVs; Gänsicke 2005). A large proportion of magnetic WDs in short-period CVs also appear to have very strong magnetic fields, exceeding 10 MG, which are much rarer in the isolated WD population.

It has also been noted that magnetic WDs appear to be rare in binary systems with a non-interacting MS companion (Liebert et al. 2005), suggesting that binary interaction may be involved in their genesis. Previous theoretical ideas have centered around the impulsive growth of a magnetic field during a binary merger (Nordhaus et al. 2007; Tout et al. 2008; Nordhaus et al. 2011). Here our focus is on a much longer-lived process that is sustained by the inward pumping of angular momentum.

A solar-mass star is slowly rotating at the end of the MS, so that the absorption of a giant planet significantly spins up the star and may trigger dynamo activity (Livio & Soker 2002). The critical planetary mass that has this effect near the base of the envelope depends on the angular velocity profile. For a flat distribution of specific angular momentum at $\text{Co} \lesssim 1$, we find that the absorption of even a Neptune-mass planet can significantly spin up the core.

A star more massive than $M_{\text{ZAMS}} \sim 1.3 M_{\odot}$ retains enough angular momentum at the end of the MS that only a planet more massive than Jupiter will significantly supplement its rotational angular momentum. Nonetheless we find that such an interaction can lead to stronger magnetic fields in the WD remnant.

Two properties of giants are especially relevant here. The inward flow of matter across the core-envelope boundary allows a net transport of magnetic helicity, which has been shown to be a necessary ingredient in the long-term stabilization of white dwarf magnetic fields (Braithwaite & Spruit 2004); and has also been implicated in the establishment of solid rotation in the radiative core of the Sun (Gough & McIntyre 1998). We show that this helicity flux can be related to the magnitude of the large-scale Maxwell torque that enforces (nearly) solid rotation in the outer core.

The outer core of an AGB star is also distinguished by an intense radiation flux. This greatly facilitates the buoyancy of a toroidal magnetic field that is anchored in a tachocline layer below the convective envelope. A thickness approaching ~ 10 percent of a scale height can maintain contact with the envelope over a dynamo period $\sim 10 - 10^2 \tau_{\text{con}}$. This suggests that a given level of magnetic activity (measured e.g. by the ratio of Maxwell to Reynolds stresses) may be achieved with a lower Coriolis parameter in an AGB envelope than in a solar-type MS star. Magnetically induced mixing of core material into the envelope (Nordhaus et al. 2008) could also be significantly enhanced by this effect.

1.2. *Remnant Spin*

The measured spins of WDs are strongly inconsistent with solid rotation in the envelope of an AGB star, combined with a tight core-envelope coupling. But even if we allow for inward convective pumping of angular momentum, the final spin rate of a WD remnant is sensitive

to the heavy loss of mass during the transition to the post-AGB phase.¹

A decoupling of the rotation of core and envelope is only feasible when the large-scale poloidal magnetic field drops below the equivalent of $10^2 - 10^3$ G in the WD during the brief, thermally pulsating AGB phase. (Much weaker fields will couple the core and envelope of a sub-giant or core helium burning star; Paper I.) This appears, at first sight, to be inconsistent with strong magnetism in the WD. In fact, a magnetic coupling between core and envelope is naturally self-limiting: once Co drops below a critical value, the dynamo operating in the inner envelope shuts off. A reasonable first guess ($\text{Co}_{\text{crit}} \sim 0.1 - 0.3$) yields WD rotation periods in the range observed in most WDs.

As a result, the remnant rotation is *inversely* correlated with the net angular momentum in the star: the slower the rotation of the AGB envelope, the sooner the decoupling between core and envelope, when the core has a larger radius and moment of inertia. The weakly magnetized surface layer of the WD is very thin, and we show that the magnetic field below quickly diffuses to the photosphere.

Our most surprising finding is that WDs with very long (\sim yr) rotation periods originate from stars which spin relatively rapidly near the end of the AGB phase. Then the rotation of core and envelope remain magnetically coupled during the contraction of the envelope. The endpoint is sensitive to details of how the envelope is expelled: in particular, to whether the envelope experiences a re-expansion following a late thermal pulse. This taps most of the remaining angular momentum of the core. Without such a re-expansion, the final rotation period can be shorter than a day.

It should be kept in mind that anisotropic contraction of the envelope can contribute to white dwarf rotation (Spruit 1998). Indeed, it may be needed to generate centrifugally supported disks that provide seeds for metal enrichment of white dwarf atmospheres.

1.3. Stellar Models and Planetary Interaction

In order to evaluate various pieces of the physics, we employ two stellar models of solar metallicity and initial mass $M_{\text{ZAMS}} = 1 M_{\odot}$ and $5 M_{\odot}$. Both models are constructed using the MESA code (Paxton et al. 2011, version 5527), with rotational degrees of freedom turned off. The normalization of the mass-loss rate on the AGB, and the masses of the WD remnants, were fixed by matching the latest initial-to-final mass relation obtained from open clusters (Dobbie et al. 2009). The coefficient entering into the formula of Blöcker (1995) was taken to be $\eta_B = 0.05$. The corresponding masses of the WD remnants are $0.55 M_{\odot}$ and $0.87 M_{\odot}$.

The rotational evolution was followed in post-processing using the rotation models described in Section 2.1. The loss of angular momentum due to mass loss on the RGB and AGB was taken into account, along with the interaction with a companion planet of a range of masses: Earth, Neptune, Jupiter in the $1 M_{\odot}$ model, and even heavier companions in the $5 M_{\odot}$ model. In the first case, the companions were started at a range of semi-major axes and orbital eccentricities. The orbit

of the planet, and the exchange of angular momentum with the star, were computed taking into account tidal drag and the gravitational quadrupole that is generated by convection in the giant envelope. Further details are given in Paper I.

1.4. Plan of the Paper

Section 2 and 3 discuss several processes that are relevant to the growth and maintenance of a stable magnetic field in the core of a post-MS star, and which determine the spin angular momentum trapped there at the end of the AGB. Section 4 presents detailed estimates of WD dipole magnetic fields. Section 5 analyzes the magnetic decoupling of core and envelope near the tip of the AGB, and provides estimates of the final WD spin. Ohmic transport through a thin, unmagnetized surface layer in a WD, and the thicker magnetized layer below it, is considered in Section 6.

Various outstanding issues – such as the sensitivity of our results to the assumed angular velocity profile in the progenitor envelope, the impulsive growth of a magnetic field during a merger, and effects associated with the anisotropic contraction of the residual AGB envelope – are addressed in the concluding Section 7. The Appendix gives further details of the accumulation of magnetic helicity in the stellar core.

2. ROTATION AND MAGNETISM IN A RAPIDLY EVOLVING GIANT STAR

Here we summarize the rotation model for giant stars that was developed in Paper I. We then review some physical constraints on generating sustainable white dwarf magnetic fields, with a focus on the accumulation of magnetic helicity during the rapid growth of the hydrogen-depleted core of a giant star. We also summarize the relative effectiveness of different convective episodes at sourcing WD magnetic fields. In this regard, there are some significant structural differences between the evolving cores of solar-mass and of intermediate-mass stars.

2.1. Combined Effect of Convection and Poloidal Magnetic Field on Angular Momentum Redistribution

Our understanding of the origin of WD rotation has been impeded by an incomplete knowledge of mixing processes in the radiative parts of the progenitor. Even a very weak poloidal magnetic field (corresponding to a magnetic field \ll MG in the WD under the assumption of magnetic flux freezing) will enforce solid rotation in the evolving core.

A popular approach recently has been to assume that such a large-scale poloidal field is initially absent, and to imagine that the radial magnetic field that is needed for angular momentum transport is generated by a current-driven (“Taylor”) instability of a predominantly toroidal field (Spruit 2002; Cantiello et al. 2014, and references therein). This leads to an incomplete coupling between core and envelope. We argue that even an inefficient dynamo process operating near the core-envelope boundary will easily short-circuit this effect.

We develop, as a working alternative, a simple and deterministic model of angular momentum redistribution in evolving stars. This model applies to stars which retain

¹ We thank Peter Goldreich for emphasizing this point to us.

(or gain) enough angular momentum to support some dynamo activity near the core-envelope boundary.

1. The outer core is assumed to rotate as a solid body, as enforced by large-scale Maxwell stresses, and to co-rotate on the average with the inner envelope.
2. Inhomogeneous rotation is sustained mainly in convective regions of the star, especially the deep outer envelope that forms following the completion of core H and He burning.

The rotation profile that is formulated and calibrated in paper I can be summarized as follows. Where the Coriolis force can be neglected, outside some transition radius R_c , the envelope maintains uniform specific angular momentum,

$$\bar{\Omega}(r) = \bar{\Omega}(R_c) \left(\frac{r}{R_c} \right)^{-2}; \quad r > R_c. \quad (2)$$

Here $\bar{\Omega}$ is the angular velocity averaged over a spherical shell. We identify R_c with the base of the envelope,

$$R_c = R_{\text{benv}} \quad (\bar{\Omega}\tau_{\text{con}} < 1 \text{ at } R_{\text{benv}}), \quad (3)$$

when the angular momentum of the star is small enough that $\bar{\Omega}(r)\tau_{\text{con}} < 1$ throughout the envelope. Throughout this paper, the subscript ‘benv’ refers to the base of the envelope.

When the star has more angular momentum, we maintain the profile (2) in the outer part of the convection zone, and consider

$$\begin{aligned} \bar{\Omega}(r) &= \bar{\Omega}(R_c) \left(\frac{r}{R_c} \right)^{-\alpha} \\ &= \frac{\text{Co}_{\text{trans}}}{\tau_{\text{con}}(R_c)} \left(\frac{r}{R_c} \right)^{-\alpha}; \quad R_{\text{benv}} < r < R_c \end{aligned} \quad (4)$$

in the inner envelope. The Coriolis parameter at the transition radius Co_{trans} is taken to be unity, and the radial index $1 < \alpha < 3/2$. As the angular momentum increases R_c moves outward, and may reach the surface of the star, in which case Co is larger than unity everywhere in the envelope.

As we discuss in Paper I, $\alpha = 1$ best matches the observed core rotation periods of sub-giant and helium burning stars, which we use to calibrate our rotational model. However, in stars of much greater size, such as those approaching the tips of the RGB and AGB, the core is more centrally concentrated and the gravitational field in the inner envelope, $g(r) \propto r^{-\beta}$, steepens from $\beta = 1$ to $\beta = 2$. Then the value of α that results from the inward transport of angular momentum by deep convective plumes increases from $(1 + \beta)/2 = 1$ to $3/2$. It is during this more advanced phase of evolution that the helicity flux into the core is expected to peak, and the rotational fate of the WD is determined. We therefore use $\alpha = 3/2$ in our analysis.

2.2. Magnetic Helicity Growth in Giant Cores

Net magnetic helicity $\mathcal{H} = \int \mathbf{A} \cdot \mathbf{B} dV$ appears to be an essential ingredient for maintaining long-term magnetostatic stability in a static and entirely fluid star (Braithwaite & Spruit 2004). Here \mathbf{B} is the magnetic

field and \mathbf{A} the vector potential from which it is derived. \mathcal{H} is a topological charge in a perfectly conducting fluid without boundary. For example, when a closed poloidal magnetic loop carrying flux Φ_p is also twisted through an angle ψ , the helicity is $\mathcal{H} = \Phi_p \Phi_\phi = \psi \Phi_p^2$, where Φ_ϕ is the toroidal flux. \mathcal{H} evolves only on a very long ohmic timescale in an extended astrophysical fluid – unless there is an exchange of magnetic twist with the exterior of the fluid, or with a medium of low electrical conductivity.

The accumulation of helicity considered here is associated with rapid changes in the structure of the star. We expect this to be possible in the outer core and inner envelope of a giant star, since this zone is connected to the surface of the star by rapid convective motions. Core convection has a topology less favorable to the accumulation of \mathcal{H} , as does the erasure of differential rotation by the stretching of magnetic field lines in the interior of a radiative star. A simplified time-dependent model of an internal shear-driven dynamo has been developed by Wickramasinghe et al. (2014), but does not address the growth of \mathcal{H} .

Such a secular accumulation of magnetic helicity – although occurring relatively rapidly near the tips of the RGB and AGB – is nonetheless a gradual process when measured over an individual dynamo cycle. There has also been longstanding interest in the role that helicity conservation may play in limiting the exponential growth of a seed magnetic field in a turbulent magnetofluid (Gruzinov & Diamond 1994; Blackman & Field 2000a; Vishniac & Cho 2001). In mean-field dynamo models, this involves a suppression of the α effect, e.g. the toroidal electromotive force which sources a large-scale poloidal magnetic field.

This limitation on fast dynamo action could be removed by the transport of magnetic helicity on a relatively short timescale, comparable to the rotation period. Such transport may involve the removal of twist across the surface of the star (Blackman & Field 2000b), or alternatively an internal flow of helicity between rotational hemispheres (Vishniac & Shapovalov 2014). In either of these cases, rapid dynamo growth is not directly dependent on changes in the net stellar helicity, obtained by summing the contribution from both hemispheres. The longer, secular effect being considered here necessarily depends on a breakdown of reflection symmetry between magnetic hemispheres; and, because it involves a change in an integral property of the star, must depend on the transport of twist across the stellar surface.

The connection between helicity growth and mass inflow can be examined with a simple model of a toroidal magnetic twist superposed on a radial magnetic field, all subjected to a radial MHD flow of speed v_r . (The sign of this flow, relative to the convective boundary, fluctuates during thermal pulses on the AGB but is negative on the average.)

Within a sphere coinciding with R_{benv} , one finds

$$\begin{aligned} \frac{d\mathcal{H}}{dt} &= \frac{d}{dt} \int \mathbf{A} \cdot \mathbf{B} dV \\ &= \frac{\partial \mathcal{H}}{\partial t} + \frac{dR_{\text{benv}}}{dt} \int dS A_\phi B_\phi = -\delta v_r \int dS A_\phi B_\phi \end{aligned} \quad (5)$$

(Appendix A). The gauge

$$A_\phi(\theta, r) = \frac{1}{r \sin \theta} \Phi_r(\theta) \quad (6)$$

is convenient, where

$$\Phi_r(\theta) = \int_0^\theta \sin \theta' r^2 B_r(\theta') d\theta' \quad (7)$$

is $(2\pi)^{-1}$ times the radial magnetic flux between the rotation axis and polar angle θ . Clearly $\Phi_r(\pi) = 0$.

One notices that the surface integral appearing in Equation (5) has the dimensions of a torque: it is comparable in magnitude to the Maxwell stress $B_r B_\phi / 4\pi$, multiplied by the lever arm $r \sin \theta$, and integrated over the core-envelope interface. Even if the net torque acting on the core boundary vanishes, $d\mathcal{H}/dt$ may remain finite as a consequence of the different angular dependences of A_ϕ and $B_r r \sin \theta$.

We are interested here in the case where $B_r B_\phi / 4\pi$ is the dominant stress driving the core material toward solid rotation. Then we can estimate the helicity flux into the core once we know the source of the Maxwell torque. The largest effect turns out to be the latitude dependence of the Reynolds stress that is applied to the core at the base of the convective envelope.

We may estimate this stress by considering a dynamo process at work in a tachocline layer right below the convective boundary. Convection above the tachocline supports strong latitudinal variations in Ω which impose a radial mis-match $\Delta\Omega$ with the mean core rotation $\Omega_{\text{benv}} = \bar{\Omega}(R_{\text{benv}})$. The tachocline can therefore be identified with the radial layer (of thickness Δr) in which $\Delta\Omega$ is concentrated,

$$\nabla\Omega \simeq \frac{\partial\Omega}{\partial r} \hat{r} \sim \frac{\Delta\Omega}{\Delta r} \hat{r}. \quad (8)$$

Our focus here is on the parts of the tachocline where $\partial\Omega/\partial r > 0$ (in the Sun, it is the equatorial band at latitudes $\lesssim 45^\circ$). The magnetorotational instability (Balbus & Hawley 1994) is excited where $\partial\Omega/\partial r < 0$, and is sustained by rapid radiative diffusion even in the presence of stable radiative convective equilibrium (Menou et al. 2004).

The poloidal magnetic field threading this part of the tachocline is wound up linearly on timescales short compared with the dynamo period P_{dyn} , which we normalize as $N_{\text{dyn}} \Delta\Omega^{-1}$. We limit the magnetic field strength in the tachocline by noting that a radial magnetic field stronger than

$$B_r \sim (4\pi\rho)^{1/2} \frac{\Delta r}{P_{\text{dyn}}} \quad (9)$$

will act to redistribute angular momentum in a layer of density ρ and thickness Δr , thereby shorting out the angular velocity gradient. The ratio of toroidal to poloidal field components is obtained from the linear winding term in the induction equation,

$$\frac{2\pi}{P_{\text{dyn}}} B_\phi \sim \frac{r \Delta\Omega}{\Delta r} B_r. \quad (10)$$

One finds that the toroidal magnetic field is in approximate equipartition with the rotational motions at the

base of the convective envelope,

$$B_\phi^2 \sim 4\pi\rho \left(r \frac{\Delta\Omega}{2\pi} \right)^2 \sim 4\pi \left(\frac{\text{Co}}{2\pi} \frac{r}{\ell_P} \frac{\Delta\Omega}{\Omega} \right)^2 \rho v_{\text{con}}^2. \quad (11)$$

The Maxwell stress works out to

$$\frac{B_r B_\phi}{4\pi} \sim \frac{\rho r \Delta r (\Delta\Omega)^2}{2\pi N_{\text{dyn}}}. \quad (12)$$

We emphasize that this estimate of the stress has been obtained from dynamical considerations, and side-steps the challenging question of how the α effect is actually manifested in a dynamo operating near a radiative-convective boundary. For recent approaches to this problem, in the context of lower-luminosity MS stars, see Blackman & Thomas (2015) and references therein.

We note that $\Delta\Omega \sim \bar{\Omega}$ is seen in anelastic calculations of deep and rapidly rotating ($\text{Co} > 1$) convective envelopes (Brun & Palacios 2009), and is suggested by the analytic treatment of angular momentum pumping in Paper I. The latitudinal gradient is milder in the Sun, where the equator rotates more rapidly than the poles, $(\Omega_{\text{eq}} - \Omega_{\text{pole}})/\bar{\Omega} \sim 0.1$; but the Solar convective envelope also has a very different aspect ratio.

Now consider the helicity flux integrated over one rotational hemisphere. Even in a state of rotational equilibrium – where the angle-integrated Maxwell torque vanishes – the integral (5) generally remains finite. Notice also that it is the product of B_r and B_ϕ that is regulated according to Equation (12). The Maxwell stress does not depend on the sign of B_r that is imposed by a dynamo operating near the core-envelope boundary, nor does it depend directly on the coherence of the magnetic field.

The sum of the two hemispheric integrals for $d\mathcal{H}/dt$ would vanish if the magnetic field were reflection-symmetric about the rotational equator. But in general it is not: the distribution of radial magnetic flux across the northern hemisphere need not precisely mirror that threading the southern hemisphere. (Only the net spherical flux vanishes.) Such an incomplete hemispheric cancellation allows a net flow of magnetic twist into the core.

Other sources of helicity flow can be considered. The inflow through the core-envelope boundary itself drives $\partial\Omega/\partial r$, but on a much longer timescale than the rotation period.

The WD magnetic fields that result from these two sources of \mathcal{H} are compared in Section 3.

2.3. Relative Importance of Different Convective Episodes

The magnetic field of a WD is influenced by a series of convective episodes in the progenitor. One measure of the relative importance of different convective episodes is provided by the convective Mach number $\mathcal{M}_{\text{con}} = v_{\text{con}}/c_s$ (here c_s is the adiabatic speed of sound), which in a stellar core can be estimated as

$$\mathcal{M}_{\text{con}} \sim \left(\frac{R_{\text{core}} v_{\text{con}}^2}{GM_{\text{core}}} \right)^{1/2}. \quad (13)$$

As the core continues to contract during later stages of nuclear burning, its magnetic energy and gravitational energy scale in the same way with central density. To

the extent that the generated Maxwell stress is limited by the convective stress, e.g. $B_\phi \lesssim (4\pi\rho)^{1/2}v_{\text{con}}$, episodes of greater \mathcal{M}_{con} are capable of generating stronger magnetic fields.

One encounters much larger \mathcal{M}_{con} on the giant branches ($\sim 10^{-3} - 10^{-2}$) than during steady core H or He burning in intermediate-mass stars ($\sim 10^{-5} - 10^{-4}$). It is also worth noting that the intense period of convection during the AGB phase is also the shortest in duration. That implies a weaker cancellation in the magnetic helicity that accumulates in the core, due to a shifting distribution of poloidal magnetic flux (see Section 2.2).

Magnetic fields that are generated during a certain convective phase will remain trapped unless exposed to later stages of convection, or the exterior mass shells are expelled. As we examine in Section 6, ohmic diffusion in the WD remnants of intermediate-mass stars is restricted to a relatively thin magnetized layer. The relevance of dynamo activity on the RGB, horizontal branch and AGB is determined, in good part, by the maximum inward penetration of the convective envelope: one requires $M(R_{\text{benv}}) \leq M_{\text{wd}}$. Only in relatively massive progenitors ($M_{\text{ZAMS}} \gtrsim 4 M_\odot$) does MS core convection extend to the mass boundary of the WD remnant, where it can influence the visible magnetic field; we ignore this effect here.

The core helium flash occurring in stars of mass $< 2.3 M_\odot$ is confined to a central subset of the eventual WD material. Because a star does not become fully convective during the flash (e.g. Bildsten et al. 2012), the magnetic helicity of the convecting core material is essentially conserved. A similar conclusion applies to the brief convective layers that are triggered by thermal pulses in the helium-burning shell near the tip of the AGB.

2.3.1. Stars with Minimal Dredge-up of Helium ($M_{\text{ZAMS}} \lesssim 2.3 M_\odot$)

In stars of initial mass $M_{\text{ZAMS}} \sim 1 M_\odot$, magnetic fields generated on the RGB are buried inside the WD remnant under a layer of CO-rich material that is produced during double shell burning (Figure 1). They are ohmically coupled on a timescale $\sim 10^8 - 10^9$ yr to a thinner magnetized shell that appears on the AGB (Section 6).

The ohmic timescale across the entire magnetized shell is longer than $\sim 10^9$ yr, meaning that any magnetic field deposited near the center of the star during the pre-MS phase would influence the surface of the star only on a timescale of a few Gyr.

We conclude that the existence of young magnetized WDs with masses $\lesssim 0.6 M_\odot$ points to dynamo activity in the convective envelope on the RGB and AGB.

2.3.2. Intermediate-mass Stars ($M_{\text{ZAMS}} \gtrsim 2.3 M_\odot$)

Stars of intermediate mass are distinguished from those of solar mass in that a dynamo operating on the RGB cannot contribute directly to the WD magnetic field: the outer parts of the helium core are dispersed by dredge up before the C/O core is assembled. In addition, only a limited mass is converted to carbon and oxygen by double shell burning (Figure 2). The fraction of the WD mass contained by this outer shell is sensitive to the rate of mass loss on the thermally pulsating AGB.

The ohmic conduction time across this outer magnetized shell is several 10^8 years. The surface magnetic field

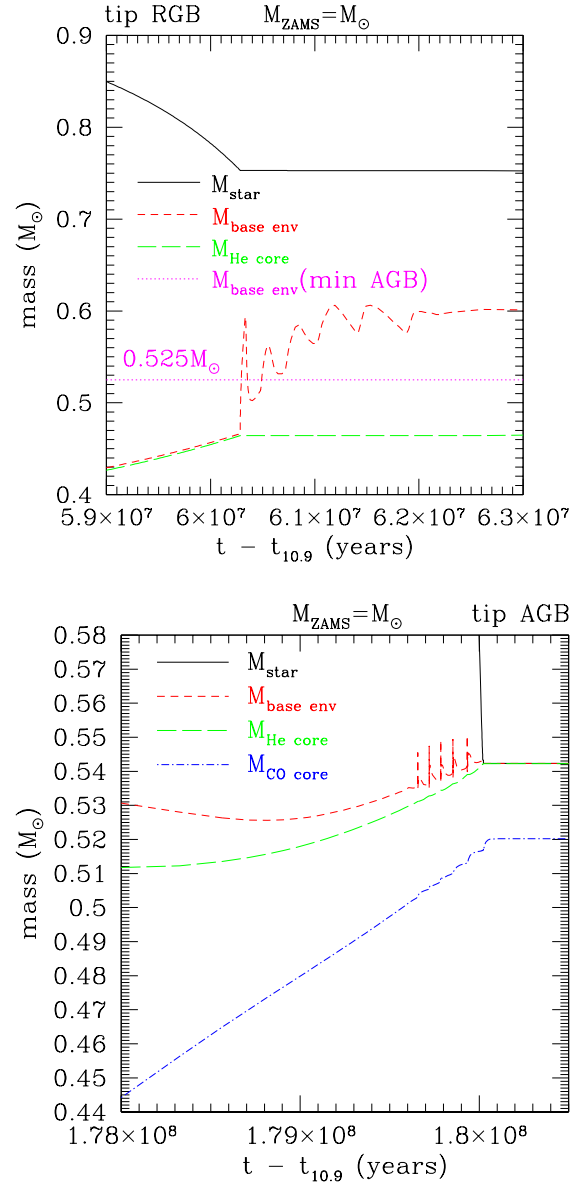


FIG. 1.— Interior profile of $M_{\text{ZAMS}} = 1 M_\odot$ star around the tip of the RGB and first stages of core He burning (top panel) and during AGB phase (bottom panel). Dotted magenta line: maximum penetration of the convective envelope on the AGB ($0.525 M_\odot$). A dynamo operating on the RGB deposits magnetized material within mass shells below this line; above it, the magnetic field is sourced on the AGB. Reference time $t_{10.9} \sim 12.37$ Gyr subtracts MS and early giant branch evolution ($R_\star(t_{10.9}) \sim 10.9 R_\odot$).

of the remnant of an isolated, intermediate-mass star is therefore expected to grow and then gradually decay on this timescale (Section 6).

3. MAGNETIC FIELD AMPLIFICATION NEAR CORE-ENVELOPE BOUNDARY

We now investigate the growth of a magnetic field above and below the core-envelope boundary of a post-MS star. There are two profound differences here with a solar-type star. First, the radiative flux that is generated by the burning shell(s) much exceeds the flux emerging from the core on the MS. Second, hydrogen-rich material drifts downward rapidly through the convective boundary, as the core grows in mass. This leads to a secular

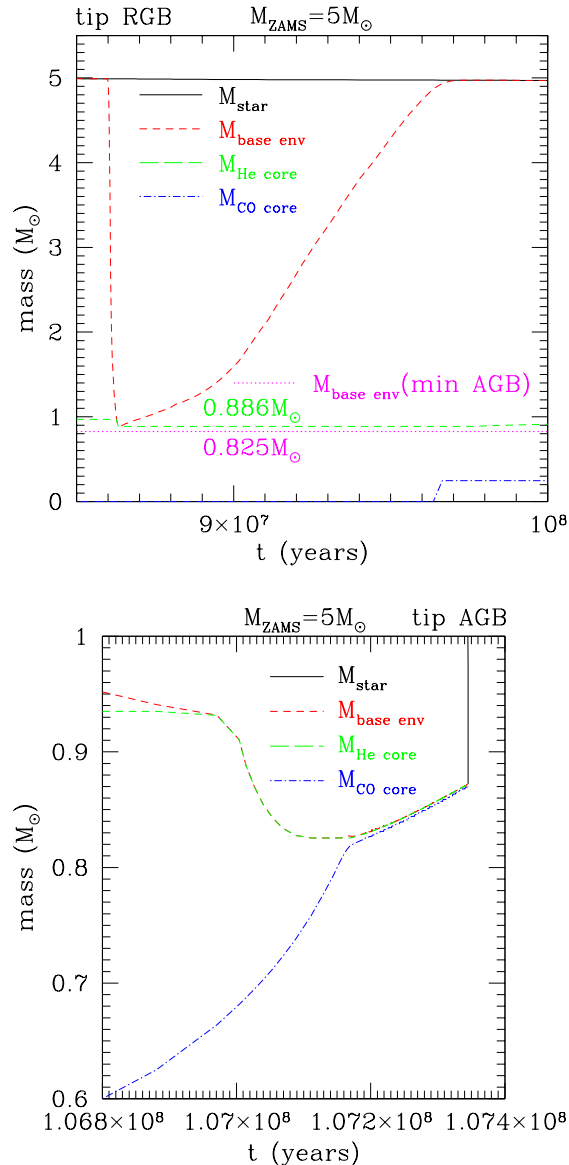


FIG. 2.— Interior profile of a $M_{\text{ZAMS}} = 5M_{\odot}$ star during RGB expansion and core He burning phase (top panel) and AGB phase (bottom panel). The deepest penetration of the convective envelope on the RGB remains outside the mass boundary of the WD remnant ($\sim 0.87M_{\odot}$). Dredge-up of helium occurs on the early AGB; the dotted magenta line shows the corresponding maximum penetration of the convection.

accumulation of magnetic helicity in the core, as this inward drift is combined with a persistent magnetic twist. Such a twist is generated when the magnetic field couples the rotation of core and envelope. In these respects, our considerations extend beyond existing dynamo theory.

3.1. Critical Co for Dynamo Action:

Effect of an Intense Radiation Flux in the Tachocline

Late-type MS stars generally are compact enough to sustain $\text{Co} \gtrsim 1$ in their convective envelopes, as are subgiants massive enough to have retained most of their natal angular momentum at the completion of core H burning. Dynamo activity, as measured by chromospheric lines and coronal X-ray emission, begins to decline when the Rossby number $\text{Ro} \equiv P_{\text{rot}}/\tau_{\text{con}} = 2\pi/\text{Co}$ is larger

than about 0.1, corresponding to $\text{Co} \lesssim 60$. Specifically in M-dwarfs, the closest MS analogs of giants, Reiners et al. (2009) observe that surface magnetic flux scales as Co^2 for $\text{Co} \lesssim 60$. There does not appear to be a sharp cut-off of magnetic activity with Coriolis parameter, as the simplest mean-field dynamo models would suggest.

The evidence therefore points to the presence of weak, but finite, dynamo activity at $\text{Co} \sim 1$ in MS stars. It also begs the question as to whether the relative strength of the dynamo-generated magnetic field (measured in terms of the convective stress at a given Coriolis parameter) differs in giants and MS stars.

First it should be emphasized that a large-scale Maxwell torque that couples the rotation of the outer core to the envelope depends on a tiny poloidal field that is implanted from the dynamo layer. We quantify this minimal field in Section 3.3.

Some additional insight is provided by mean-field dynamo theory, which suggests that the dynamo number

$$D \equiv \frac{\alpha \Omega r^3}{\nu_t^2} \sim \left(\frac{\alpha}{v_{\text{con}}} \right) \left(\frac{r}{\ell_P} \right)^3 \text{Co} \quad (14)$$

must exceed a threshold $D \gtrsim (2\pi)^3 \sim 10^2$ for magnetic field growth to be sustained (Charbonneau 2014). Here α is the parameter relating the toroidal magnetic field to the toroidal electromotive force, and ν_t is the turbulent diffusivity. The prospect for a dynamo is enhanced if the magnetic field can be anchored in a part of the star with relatively low (but finite) ν_t .

This effect provides part of the motivation for considering a thin, stably-stratified layer below the convective envelope as the locus of strong differential rotation, and a reservoir for a toroidal magnetic field (Parker 1993). However, the sharpness of the onset of stable stratification below the envelope boundary has presented a difficulty for this hypothesis. The solar convective motions have a relatively low Mach number ($\mathcal{M}_{\text{con}} \sim 10^{-4}$), and so the overshoot layer below the envelope is very thin. A toroidal magnetic field reaching equipartition with the convective stresses overcomes the stable stratification in a layer that is not much thicker.

In Section 3.2, we show that the intense flux of radiation emanating from the core of a RGB or AGB star will induce an upward drift of magnetized material, one that more than counterbalances the downward flow to the burning shell(s). A tiny seed field that is generated by the convective motions will sustain this feedback (Section 3.3). The interchange between toroidal and poloidal fields will persist in a layer of considerable thickness $\sim (0.01 - 0.1)\ell_P$ over a dynamo cycle $\sim (10 - 10^2)\tau_{\text{con}}$. Convectively driven turbulence is strongly suppressed within this layer.

3.2. Magnetic Buoyancy in the Tachocline

We now examine the competition between the downward drift of hydrogen-rich material across the tachocline, and the upward drift of magnetized material (Figure 3). Consider a horizontal (toroidal) magnetic flux tube, of a radial thickness comparable to the distance $\Delta r = R_{\text{benv}} - r$ to the base of the convective envelope. The flux tube starts in buoyancy equilibrium, with a density equal to that of its unmagnetized surroundings.

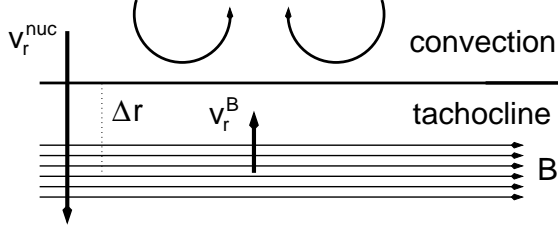


FIG. 3.— A magnetic flux tube positioned in the tachocline layer experiences an upward drift that is driven by the intense radiation flux through the tube. This drift can be strong enough to counterbalance the downward flow of hydrogen-rich material into the burning shell(s) below.

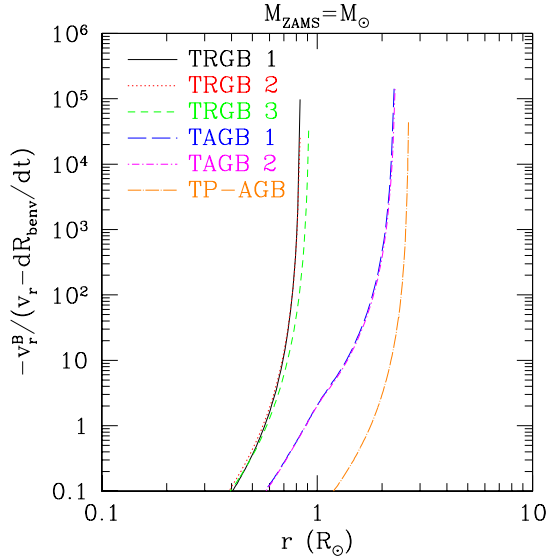


FIG. 4.— Horizontal (toroidal) magnetic field anchored in a tachocline experiences radiatively driven buoyancy. Upward drift speed v_r^B , Equation (19), is compared with the downward flow of material from the convective envelope into the growing radiative core. Curves correspond to various timesteps near the tips of the RGB and AGB in our $1 M_\odot$ model, and one taken from the thermally pulsating AGB. The magnetic field is normalized to $B_\phi \sim (4\pi\rho v_{\text{con}}^2)^{1/2}$, with v_r^B proportional to B_ϕ^2 . Buoyant drift accelerates toward the core-envelope boundary, due to the decrease in the Brunt-Väisälä frequency. Here downflow is evaluated directly from the stellar model.

The temperature deficit in the flux tube (labelled ‘B’) is

$$\frac{T_B - T}{T} = -\frac{B_\phi^2}{8\pi P}, \quad (15)$$

which maintains a differential energy flux

$$\delta F_{\text{rad}} \sim -\frac{4ac}{3\kappa\rho\Delta r}(T_B - T)T^3 \quad (16)$$

into the flux tube. This drives a buoyant rise of the flux tube at a speed v_r^B , which is determined by

$$\rho k_B T v_r^B \frac{dS}{dr} = -\frac{dF_{\text{rad}}}{dr} \sim \frac{\delta F_{\text{rad}}}{\Delta r}. \quad (17)$$

The background entropy gradient is usefully expressed in terms of the Brunt-Väisälä frequency

$$N = \sqrt{g \frac{\gamma - 1}{\gamma} \frac{dS}{dr}}, \quad (18)$$

so that

$$v_r^B \sim \left(\frac{B_\phi^2}{8\pi P} \right) \frac{F_{\text{rad}}}{(\Delta r)^2 \rho N^2}. \quad (19)$$

The background flow of mass into the radiative core is

$$\frac{dM_{\text{core}}}{dt} = 4\pi R_{\text{benv}}^2 \rho(R_{\text{benv}}) \left(\frac{dR_{\text{core}}}{dt} - v_r^{\text{nuc}} \right) \sim \frac{L}{\varepsilon_i}. \quad (20)$$

After the star passes onto the thermally pulsating AGB, the relation between core growth rate and luminosity L only holds after averaging over pulsations. The nuclear energy released per unit mass of new core material is $\varepsilon_1 = 6.3X \text{ MeV}/m_u$ during the first step of converting material with hydrogen mass fraction X to helium; and $\varepsilon_2 = \varepsilon_1 + 0.8 \text{ MeV}/m_u$ during double shell burning. The corresponding velocity is

$$v_r^{\text{nuc}} \sim -\frac{F_{\text{rad}}}{\rho \varepsilon_i}. \quad (21)$$

The ratio $v_r^B/|v_r^{\text{nuc}}|$ is plotted in Figure 4 at various intervals during the RGB and AGB evolution of our $1 M_\odot$ model. One observes that the most strongly magnetized parts of the tachocline will not be subducted if the magnetic pressure approaches the kinetic pressure at the base of the convective envelope. It should be kept in mind that this effect depends on a difference in magnetization: subduction of the less weakly magnetized parts of the tachocline must continue even where $v_r^B > |v_r^{\text{nuc}}|$.

Magnetic buoyancy has the effect of expanding the active dynamo region below R_{benv} , by allowing a layer with strong $d\Omega/dr$ – the tachocline – to remain in contact with the convection zone.² We can estimate the size of this region by comparing the buoyant rise time $\Delta r/v_r^B(r)$ with the dynamo timescale P_{dyn} (set equal to $100\tau_{\text{con}}$)

$$\Delta r \equiv R_{\text{benv}} - r = v_r^B(r) \cdot P_{\text{dyn}}. \quad (22)$$

To invert this expression, we fit $v_r^B(\Delta r)$ to a power law in Δr , measuring it in two different radial zones.

Figure 5 shows the resulting buoyant shell thickness, in comparison with the local scale height, during the AGB phase of the $5 M_\odot$ model. The buoyant shell thickness reaches $\sim 0.1P(R_{\text{benv}})$ before and during the first thermal pulse, and then relaxes to a value about 10 times smaller.

3.3. Seeding a Toroidal Magnetic Field in the Tachocline

We now consider the minimal seed field that will trigger dynamo feedback in the tachocline, thereby facilitating the magnetic coupling of core and envelope. We suppose

² We do not address here whether the re-conversion of wound toroidal magnetic field back to the poloidal direction is concentrated in the tachocline, or instead the convection zone, as in Parker’s 1993 model.

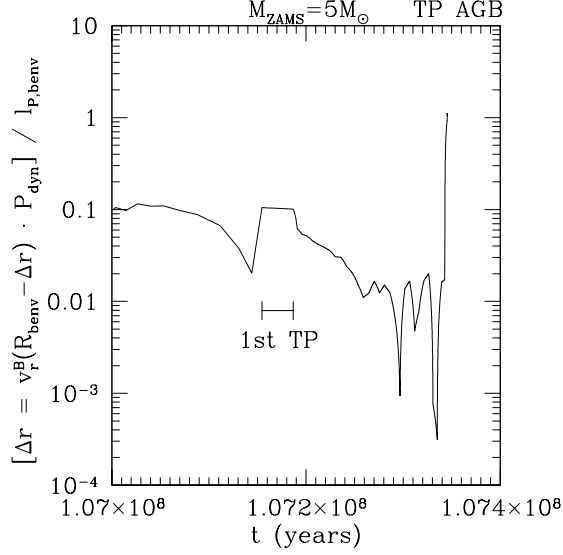


FIG. 5.— Thickness Δr of magnetized shell below the core-envelope boundary which remains in contact with the inner convection zone over the dynamo period P_{dyn} . See Equation (22). Here Δr is normalized to the local pressure scaleheight. Plot covers the thermally pulsating AGB phase of the $5 M_{\odot}$ model, with $B_{\phi} = (4\pi\rho v_{\text{con}}^2)^{1/2}$.

that this seed field is generated within the convective envelope, and is deposited in the outer radiative core by the mass flow toward the burning shell(s).

This seed field must pass a certain threshold if linear winding in the tachocline is to generate a buoyantly unstable toroidal field. The time available for linear winding depends on the depth Δr below the radiative-convective boundary. Consider an unmagnetized core in which matter flowing across the convective boundary sustains an angular velocity profile $\Omega = \Omega_{\text{benv}}(r/R_{\text{benv}})^{-2}$. Near the boundary, the toroidal magnetic field that is sourced by a seed radial field B_{seed} is $B_{\phi} = -2B_{\text{seed}}\Omega_{\text{benv}}\Delta r/v_r^{\text{nuc}}$. Substituting this into Equation (19) and setting $v_r^B > |v_r^{\text{nuc}}|$ gives

$$\frac{B_{\text{seed}}^2}{4\pi\rho(R_{\text{benv}})v_{\text{con}}^2} > \frac{N^2}{2\Omega^2} \frac{P|v_r^{\text{nuc}}|^3}{v_{\text{con}}^2 F_{\text{rad}}}. \quad (23)$$

This minimal seed field for dynamo feedback turns out to be quite weak. Figure 6 shows $B_{\text{seed}}/\sqrt{4\pi\rho(R_{\text{benv}})v_{\text{con}}}$ during the final AGB evolution of a $5 M_{\odot}$ star, measured at a distance $\Delta r = l_P(R_{\text{benv}})/10$ below the core-envelope boundary. Much of the C/O mass deposition from double shell burning is concentrated around $t \sim 1.0716 \times 10^8$ yr, when this quantity is as small as $\sim 10^{-9}$; it rises to $\sim 10^{-4}$ during the phase of rapid thermal pulses.

Hydrodynamic turbulence is strongly suppressed in the tachocline. The mean-field approach to dynamo action then suggests (see the review in Section 3.1) that dynamo activity should be easily sustained in the tachocline as long as the toroidal magnetic field can be rotated back into the poloidal direction. This effect is present in numerical simulations of a shear layer (Cline et al. 2003); and is conjectured to operate in a more global dynamo model where toroidal magnetic field formed in the tachocline diffuses into the convective envelope (Parker

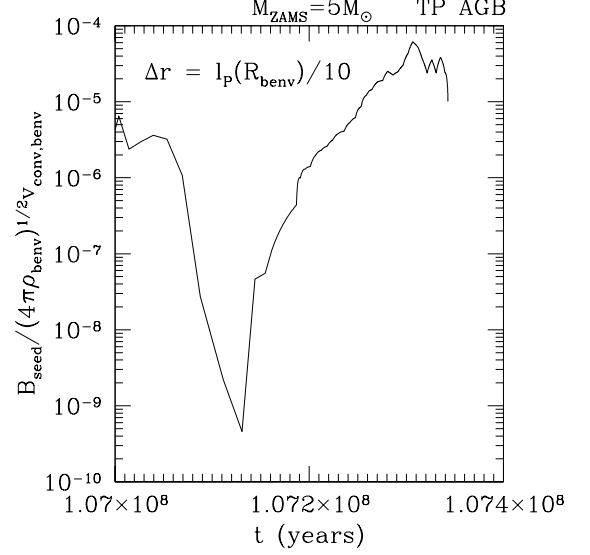


FIG. 6.— Minimal seed poloidal magnetic field, deposited in the outer core of an AGB star, which will grow by linear winding to a sufficient strength that radiatively driven magnetic buoyancy overcomes the downward drift of envelope material to the burning shell(s). Equation (23) is evaluated at depth $\Delta r = l_{P,\text{benv}}/10$ below core-envelope boundary. Plot covers same thermally pulsating AGB phase of $5 M_{\odot}$ model as Figure 5.

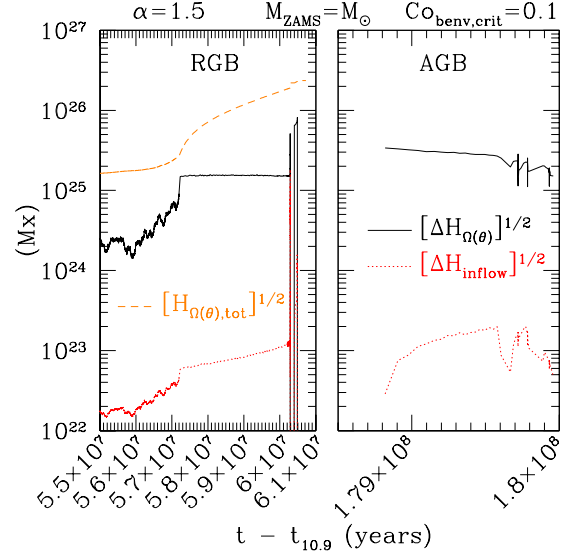


FIG. 7.— The magnetic helicity (expressed as a magnetic flux $\Delta\mathcal{H}^{1/2}$) that accumulates in the time $t_{\text{drift}} = \ell_P/|v_r^{\text{nuc}}|$. RGB (left) and AGB (right) evolution of $M_{\text{ZAMS}} = 1 M_{\odot}$ model with a Jupiter companion in an initial orbit $a_i = 1$ AU. Most of the helicity generated on the RGB is concentrated near the tip (orange short-dash curve shows cumulative helicity). This gives $M_{\text{benv}}(5.65 \times 10^7) \sim 0.388 M_{\odot}$ as the effective base of the magnetized region. The net mass passing through the dynamo-active layer is then $\sim 0.12 M_{\odot}$ on the RGB, and $\sim 0.014 M_{\odot}$ on the AGB. The greater helicity accumulated through the ‘ $\Omega(\theta)$ ’ channel (Equation (27)), as compared with the ‘inflow’ channel (Equation (33)), is reflected in the final WD magnetic field (Figure 9).

1993). Estimates of the equipartition toroidal magnetic field and the large-scale Maxwell stress are given by equations (11) and (12).

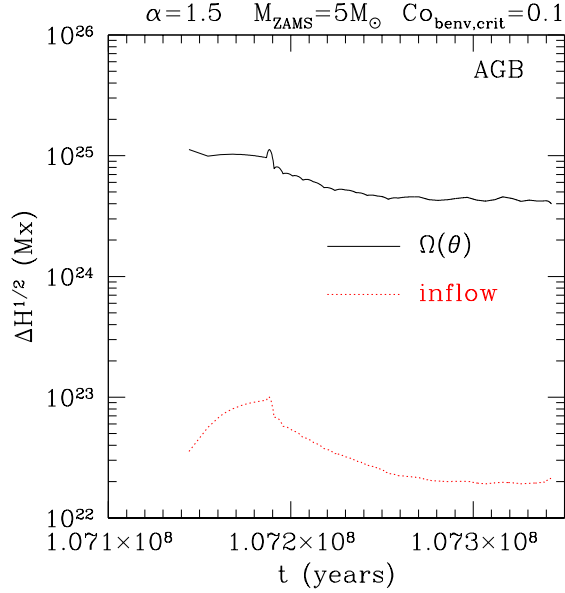


FIG. 8.— Comparison of magnetic helicity generated over $t_{\text{drift}} = \ell_P/|v_r^{\text{nuc}}|$ through the same two channels as Figure 7, but now in the $M_{\text{ZAMS}} = 5 M_{\odot}$ model without a planetary companion. Only the AGB contributes directly to final WD magnetization in this case, within a mass shell $\sim 0.044 M_{\odot}$. The largest net contribution comes from the first thermal pulse.

4. WHITE DWARF MAGNETIC FIELD

After magnetic helicity accumulates in the core, we allow the magnetic field to relax to a more isotropic configuration. A first estimate of the flux threading one hemisphere is

$$\Phi_{\text{core}} \simeq \mathcal{H}^{1/2}. \quad (24)$$

The final poloidal magnetic field of a WD of radius R_{wd} is

$$B_{\text{wd}} \sim \frac{\Phi_{\text{core}}}{\pi R_{\text{wd}}^2}. \quad (25)$$

We first evaluate the magnetic helicity that is deposited in a post-AGB star, using the $1 M_{\odot}$ and $5 M_{\odot}$ stellar models constructed using MESA. This stored helicity is then converted to a dipolar magnetic field in the WD remnant using Equations (24) and (25).

This estimate presupposes that toroidal and poloidal magnetic fluxes evolve to an energy minimum with $\Phi_p \sim \Phi_\phi$, all the while preserving the product helicity $\mathcal{H} \sim \Phi_p \Phi_\phi$. Such an interchange may occur later in the life of a WD as the result of ohmic diffusion (Section 6); or earlier on as the result of relaxation within episodes of confined convection (such as the core helium flash, or helium shell flashes).

4.1. Accumulation of Magnetic Helicity in a Radiative Core Relaxing to Solid Rotation

The zone of interest here is the tenuous mantle of radiative material that is sandwiched between the hydrogen-depleted core and the base of the convective envelope. Here only a small mass $\lesssim 10^{-3} M_{\odot}$ lies within a scale-height, and so we model the mass inflow through the mantle as quasi-steady,

$$\dot{M}_{\text{core}} = 4\pi r^2 |v_r| \rho(r). \quad (26)$$

The poloidal magnetic field is approximated as radial with flux function (7), and the toroidal magnetic field is expressed in terms of a radial magnetic twist as $B_\phi(r, \theta) = (\partial \phi_B / \partial r) r \sin \theta B_r$. Then helicity accumulates in the core at the rate

$$\frac{d\mathcal{H}}{dt} = -2\pi \delta v_r \int d\theta \Phi_r \frac{\partial \Phi_r}{\partial \theta} \frac{\partial \phi_B}{\partial r}, \quad (27)$$

where δv_r is the flow velocity relative to the core-envelope boundary.

Now consider the torque imparted to a mass shell by the Maxwell stress $B_r B_\phi / 4\pi$,

$$\frac{d}{dt} \left(\delta m \frac{2}{3} r^2 \bar{\Omega} \right) = \delta \left[\int dS r \sin \theta \frac{B_r B_\phi}{4\pi} \right]. \quad (28)$$

Here the Lagrangian time derivative follows the radial flow at speed v_r . Since $d(\delta m)/dt = 0$, one has, following Equation (7),

$$\frac{d}{dt} \left(\frac{2}{3} r^2 \bar{\Omega} \right) = \frac{1}{8\pi \rho r^2} \int d\theta \sin \theta \left(\frac{\partial \Phi_r}{\partial \theta} \right)^2 \frac{\partial^2 \phi_B}{\partial r^2}. \quad (29)$$

Both hemispheres generally contribute in the same sense to the torque.

4.1.1. Helicity Sourced by Radial Inflow

We suppose that the magnetic field is strong enough that nearly solid rotation is maintained in the radiative layers, $|\partial \Omega / \partial r| \ll \bar{\Omega} / r$. Each mass shell starts with a mean angular frequency Ω_{benv} that is imposed by the lower part of the convective envelope. The twist that is required to maintain a weak angular velocity gradient is found from Equation (29),

$$\frac{\partial^2 \phi_B}{\partial r^2} \sim -\frac{2\dot{M}_{\text{core}} \Omega_{\text{benv}} r}{(B_r r^2)^2}, \quad (30)$$

where the coefficient on the right-hand side corresponds to B_r independent of θ . From Equation (A10) one has

$$\frac{\partial \phi_B}{\partial r} \sim \frac{r}{|v_r|} \frac{\partial \Omega}{\partial r}. \quad (31)$$

Nearly solid rotation is maintained if

$$v_{A,r}^2 \equiv \frac{B_r^2}{4\pi \rho} \gg v_r^2. \quad (32)$$

Now consider the magnetic helicity that is advected into the growing radiative core. We evaluate the magnetic twist in Equation (27) from Equation (30), obtaining

$$\frac{d\mathcal{H}}{dt} = f(\Delta M_{\text{core}}) \cdot \pi \dot{M}_{\text{core}} \Omega_{\text{benv}} R_{\text{benv}}^2 \delta v_r(R_{\text{benv}}) \quad (33)$$

at $r = R_{\text{benv}}$.

The factor f , with indeterminate sign but magnitude $|f| < 1$, represents the cancellation between hemispheres. We discuss its origin in Section 4.1.3.

4.1.2. Magnetic Twist Compensating a Latitude-dependent Convective Torque

A greater Maxwell stress results from the application of convective stresses to the outer radiative core. A convection zone generally sustains latitudinal gradients in

rotation. Part of the differential Reynolds stress is transmitted through the tachocline to the core by a dynamo-generated magnetic field (Equation (12)). As a working estimate, we use

$$\frac{B_r B_\phi}{4\pi} = \varepsilon_B \rho(R_{\text{benv}})(\Omega_{\text{benv}} R_{\text{benv}})^2, \quad (34)$$

with $\varepsilon_B \sim 10^{-3}$, corresponding to a dynamo period $P_{\text{dyn}} \sim 10[\Delta\Omega(R_{\text{benv}})]^{-1}$ and a pole-equator offset $\Delta\Omega(R_{\text{benv}}) \sim \Omega_{\text{benv}}$.

Given that the deeper parts of the radiative core are coupled magnetically to the tachocline, uniform rotation can be maintained in the outer core only if this stress is divergence-free below the tachocline. The corresponding magnetic helicity flow into the core through the advection of this twisted field is

$$\frac{d\mathcal{H}}{dt} = f(\Delta M_{\text{core}}) \cdot \pi \varepsilon_B \dot{M}_{\text{core}} R_{\text{benv}} (\Omega_{\text{benv}} R_{\text{benv}})^2. \quad (35)$$

The contributions to \mathcal{H} from equations (33) and (35) are labelled in the Figures as ‘inflow’ and ‘ $\Omega(\theta)$ ’, respectively.

4.1.3. Cancellation Between Hemisphere

One feature of Equations (33) and (35) stands out: the growth of \mathcal{H} is independent of the seed radial magnetic field, as long as it is strong enough to satisfy the inequality (32). This means that the contribution to $\mathbf{A} \cdot \mathbf{B}$ in one hemisphere is not strongly affected by fluctuations in the magnitude and sign of the poloidal magnetic field that is supplied to the radiative layer by a dynamo operating near the convective boundary.

A net mass ΔM_{core} flows through the convective-radiative boundary over the duration of dynamo activity. In the case of an AGB star, this is approximately the increase in the mass of the C/O core due to double-shell burning. Note that ΔM_{core} is generally much larger than the mass of the rarefied core mantle ($\sim 10^{-3} M_\odot$). The low mass of the mantle imposes a short-timescale cutoff to fluctuations in the summed \mathcal{H} from the two hemispheres. We express this cutoff in terms of the mass within a scale height below the core-envelope boundary,

$$\Delta M_{\text{min}} \sim \frac{4\pi P r^4}{GM_{\text{core}}} \Big|_{R_{\text{benv}}}. \quad (36)$$

Then we take

$$f(\Delta M_{\text{core}}) \sim \left(\frac{\Delta M_{\text{min}}}{\Delta M_{\text{core}}} \right)^{1/2}. \quad (37)$$

4.2. Results

First consider the $M_{\text{ZAMS}} = 1 M_\odot$ model. The angular momentum profile of the star is evolved in post-processing using the method of Section 2.1 and Paper I. Companion planets with a range of masses (Earth, Neptune, and Jupiter) are placed at an initial semi-major axis $a_i = [0.5, 0.75, 1, 1.5, 2]$ AU and with a range of orbital eccentricities.

Magnetic fields generated during the RGB and AGB phases both contribute to the remnant WD field, but at different depths in the star (see Figure 1). A net mass $\sim 0.135 M_\odot$ passes through the core-envelope boundary

while conditions are favorable for magnetic field growth.³

Figure 7 shows the helicity that accumulates in the brief period $t_{\text{drift}} = \ell_P / |v_r^{\text{nuc}}|$ when stellar material settles through the outer scale height of the radiative core. The dominant contribution comes from the ‘ $\Omega(\theta)$ ’ channel.

In the $5 M_\odot$ star, only helicity accumulated on the AGB contributes directly to the final WD magnetic field (Figure 2). During this phase $\sim 0.044 M_\odot$ passes through the active dynamo region (given our normalization $\eta_B = 0.05$ of the Blöcker mass loss formula). We see in Figure 8 that the initial phase of the dynamo, which occurs during the first thermal pulse, contributes the majority of \mathcal{H} . In the $5 M_\odot$ model, we simplified the treatment of the thermal pulses by linearly interpolating all of the relevant quantities between the local minima in R_{benv} after each He shell flash, so as to focus on the mean growth of core mass and \mathcal{H} . The stellar model considered in Figure 8 has no planetary companion.

The resulting WD dipolar field is shown in Figure 9 for both the $1 M_\odot$ and $5 M_\odot$ models, using the mass-radius relation of Zepolsky & Salpeter (1969). A strong magnetic field in the $0.55 M_\odot$ WD remnant of the $1 M_\odot$ progenitor depends on the injection of angular momentum from a planetary companion (as considered here), or a tidal interaction with a stellar companion. We find that B_{wd} is an increasing function of the angular momentum absorbed; the various points correspond to different realizations of the orbital evolution.

Dipole fields approaching 10^8 G are achievable through the ‘ $\Omega(\theta)$ ’ channel, following the absorption of a Jupiter-mass planet. Note that an Earth-mass planet does not significantly augment the angular momentum left over at the end of the MS spindown, and so this case corresponds closely to an isolated star that does not interact with planets.

Figure 9 focuses on those runs which end in the engulfment of the planet. However there are cases in which the planet is pushed out into a large orbit due to the convective quadrupole. The planet therefore gains angular momentum from the star, which in turn causes the star to spin in the opposite direction. In some cases this leads to the development of a dynamo as well. We ignore these particular cases.

An external source of angular momentum injection is not required to sustain a dynamo in the $5 M_\odot$ progenitor. Nonetheless, B_{wd} depends on the C/O mass that accumulates during double shell burning, and therefore on the mass-loss rate during the expulsion of the envelope.

The effect of adding a relatively massive companion to the $5 M_\odot$ model is considered in Figure 10. The absorption of a $3 M_J$ planet significantly augments the remnant dipole field in the $0.87 M_\odot$ WD. We see a steady increase in the remnant field as the companion mass increases to the brown dwarf range, or even to $\sim 0.1 M_\odot$, for the angular velocity profile considered here ($\alpha = 3/2$). For comparison we show the magnetic fields obtained by a shallower inner rotation profile ($\alpha = 1$), which may be applicable depending on the strength of the Coriolis back reaction. In this case an increase in angular momentum

³ For example, we do not include the first dredge-up phase, during which the convective envelope grows in mass.

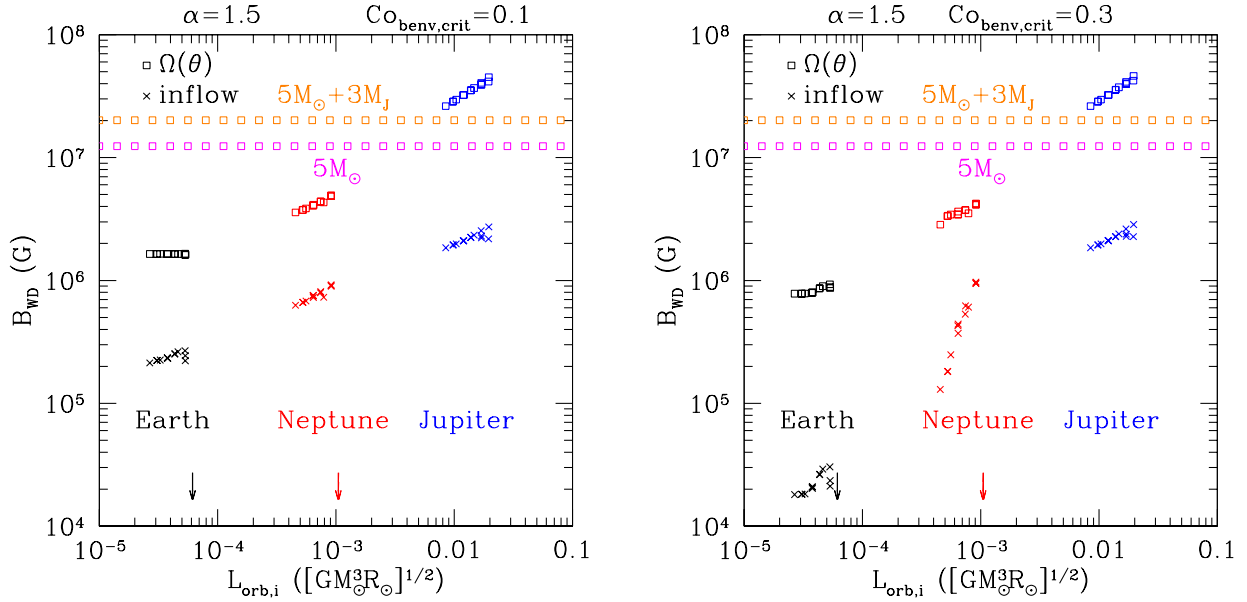


FIG. 9.— Dipole magnetic field, Equation (25), left behind in the WD remnant of a $1 M_{\odot}$ star interacting with a planet (black = Earth mass, red = Neptune mass, blue = Jupiter mass). Result is plotted separately for the two helicity channels described in the text. Horizontal axis shows initial orbital angular momentum of planet companion. Each tick represents an average over realizations of a given set of orbital initial conditions (a_i and e_i). Magenta squares show result for $5 M_{\odot}$ progenitor with initial equatorial rotation speed 50 km s^{-1} and no companion; orange squares same model with angular momentum of $3 M_J$, $a_i = 2 \text{ AU}$ planet added during early AGB. Dynamo shuts off when $\text{Co}_{\text{benv}} < \text{Co}_{\text{benv,crit}} = 0.1$ (left panel) or $\text{Co}_{\text{benv,crit}} = 0.3$ (right panel).

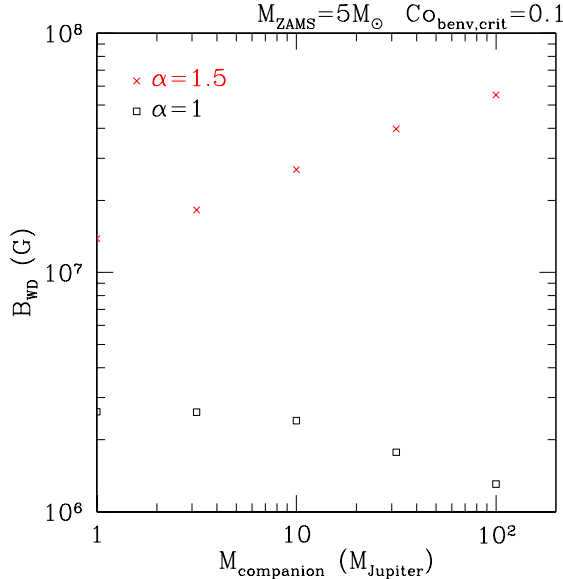


FIG. 10.— Dipole magnetic field obtained via the $\Omega(\theta)$ channel in the $0.87 M_{\odot}$ remnant of a $5 M_{\odot}$ star that absorbs an orbiting companion ($a_i = 2 \text{ AU}$) of various masses during the early AGB phase ($R_{\star} = 200 R_{\odot}$). Top points: rotation profile $\Omega(r) \propto r^{-1.5}$ (r^{-2}) in the inner (outer) convective envelope ($\alpha = 1.5$ in Equation (4)). Bottom points: $\alpha = 1$.

results in a decrease of remnant magnetic field, caused by a decrease in Co_{benv} due to the shallow $\tau_{\text{conv}}(r)$ profile.

5. WHITE DWARF ROTATION

We now analyze the spin evolution of the core and envelope of our stellar models. Our focus is on the magnetic *de*-coupling between the core and envelope. Three factors determine the effectiveness with which a poloidal

magnetic field transfers angular momentum across the core-envelope boundary, and establishes solid rotation in the outer core: i) the timescale over which mass is exchanged between core and envelope; ii) the direction of this exchange; and iii) the Coriolis parameter in the inner envelope.

The internal structure of the star evolves slowly enough during the early ascent of the giant branches, and during core helium burning, that a magnetic coupling between core and envelope is very difficult to avoid (see Figure 2 of Paper I). There is a much more rapid exchange of mass between envelope and core near the tips of the RGB and AGB. The first giant phase is (except in cases of close binary interaction) followed by more extended evolution. So our focus here is on the final AGB superwind phase during which most of the envelope mass is removed.

The ability of the inner envelope to generate a magnetic field is most relevant while the radiative core is growing in mass. Then magnetized material is advected downward into the outer core, where it can communicate changes in rotation rate in the envelope to the inner core. The core grows in mass during the thermally pulsating AGB phase, after averaging over the pulsations; but following the contraction of the envelope the superwind causes a small but rotationally significant decrease in mass.

An important effect involves the re-expansion of the envelope following a late thermal pulse: following this about $10^{-3} M_{\odot}$ of hydrogen-rich material is transferred to the convective envelope. If core and envelope are still magnetically coupled, this causes a dramatic spindown of the core through the internal exchange of angular momentum.

Faster WD spin is mediated by an early loss of angular momentum from the surface of an AGB star. This loss,

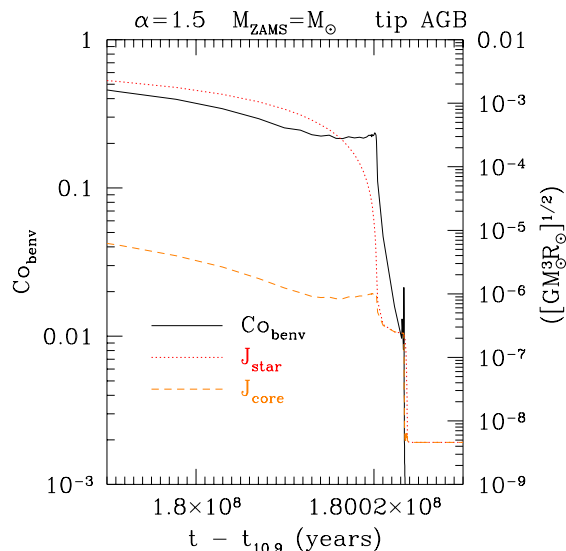


FIG. 11.— Rotational angular momentum of $M_{\text{ZAMS}} = 1 M_{\odot}$ AGB star (dotted red line) and its core (short-dash orange line) just before and during the super-wind phase. The star has absorbed a Jupiter-mass companion near the tip of the RGB. Black line: Coriolis parameter at base of convective envelope. Rotation profile $\Omega(r) \propto r^{-1.5}$ (r^{-2}) in the inner (outer) convective envelope. When calculating remnant WD spins, we freeze Ω_{core} when and if Co_{benv} drops below a critical value, beyond which time the curves plotted here do not apply.

if strong enough, will push the Coriolis parameter Co_{benv} of the inner envelope below unity well before the envelope contracts. The remnant WD spin period depends on the critical value of Co_{benv} below which the dynamo effectively shuts off. If the transition to $\text{Co}_{\text{benv}} < \text{Co}_{\text{benv,crit}}$ takes place before the final shell flash, then the angular momentum of the core is effectively frozen in and inherited by the WD. On the other hand, if this transition occurs afterward, then we expect that the rotation of the outer core remains coupled to the inner envelope as the photosphere of the star contracts.

Figures 11 and 12 show the evolution of the net stellar angular momentum J_{\star} and the core angular momentum J_{core} during the AGB phase, under the assumption of a tight core-envelope coupling. The internal rotation profile, the prescription for mass and angular momentum loss, and the interaction with a planetary companion, are the same as those described in Sections 1 & 2 and detailed in Paper I. As the star experiences strong mass loss, there is a rapid drop in J_{\star} .

During this phase, J_{\star} is still dominated by the envelope. Also plotted is Co_{benv} for comparison. Core-envelope decoupling becomes plausible at $\text{Co}_{\text{benv}} = \text{Co}_{\text{benv,crit}} \sim 0.1\text{--}0.3$, given the strong dependence of magnetic field on rotation that is observed in deeply convective MS stars (Reiners et al. 2009).

Whether the transition to $\text{Co}_{\text{benv}} < \text{Co}_{\text{benv,crit}}$ is encountered before the final He shell flash depends on both J_{\star} and the value of $\text{Co}_{\text{benv,crit}}$. The transition occurs earlier for a larger critical Coriolis parameter, as in our $1 M_{\odot}$ model with $\text{Co}_{\text{benv}} = 0.3$. But we find a tighter restriction on J_{\star} when Co_{benv} is reduced to 0.1: then the absorption of a Jupiter will cause core and envelope to remain coupled past the final flash in the $1 M_{\odot}$ model, but the absorption of a Neptune (or of no planet) al-

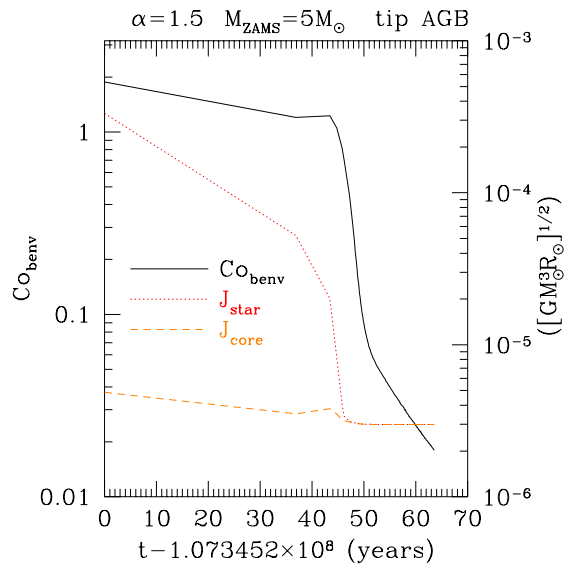


FIG. 12.— Similar to Figure 11, but for the $M_{\text{ZAMS}} = 5 M_{\odot}$ star.

lows a transition to a weakly magnetized envelope. We find that Co_{benv} generally remains above $\text{Co}_{\text{benv,crit}}$ at the final shell flash in the $5 M_{\odot}$ model, implying a tight core-envelope coupling during the transition to a post-AGB star.

In the following two sections, we separately consider the rotational evolution of our stellar models with, and without, a transition to weak core-envelope coupling.

5.1. Dependence of White Dwarf Spin on Coriolis Parameter for Core-Envelope Decoupling

The WD spin period that results from core-envelope decoupling at $\text{Co}_{\text{benv,crit}} = 0.1$ and 0.3 in the $1 M_{\odot}$ model is shown in Figure 13. For the more conservative estimate $\text{Co}_{\text{benv,crit}} = 0.1$, we find that P_{wd} ranges over $0.5\text{--}1.5$ d.

In this situation, where the timing of the transition to weak magnetization in the envelope depends on J_{\star} , P_{wd} depends on the initial orbital angular momentum of the planetary companion. A lower total angular momentum results in faster decoupling, and therefore a *larger* trapped core angular momentum: the core rotation frequency at decoupling is tied to the convective timescale in the inner envelope, and to the structure of the star.

This behavior is explained in Figure 14, which shows the minimum angular momentum required to maintain $\text{Co}_{\text{benv}} = 0.1$ in the $1 M_{\odot}$ model near the tip of the AGB. This is compared with the actual angular momentum evolution that results from the absorption of a Jupiter, Neptune or Earth, initially orbiting at $a_i = 1$ AU with eccentricity $e_i = 0$.

5.2. White Dwarf Spin in Case of Continued Core-Envelope Coupling

We observe a significant difference in the remnant angular momentum in two models which maintain a tight core-envelope coupling through to the post-AGB phase: the $5 M_{\odot}$ model, and the $1 M_{\odot}$ model which absorbs a Jupiter-mass planet. In the first case, downward angular momentum pumping in the convective envelope allows J_{core} to remain relatively constant during the ejection of the envelope, and only modest spindown is caused by a

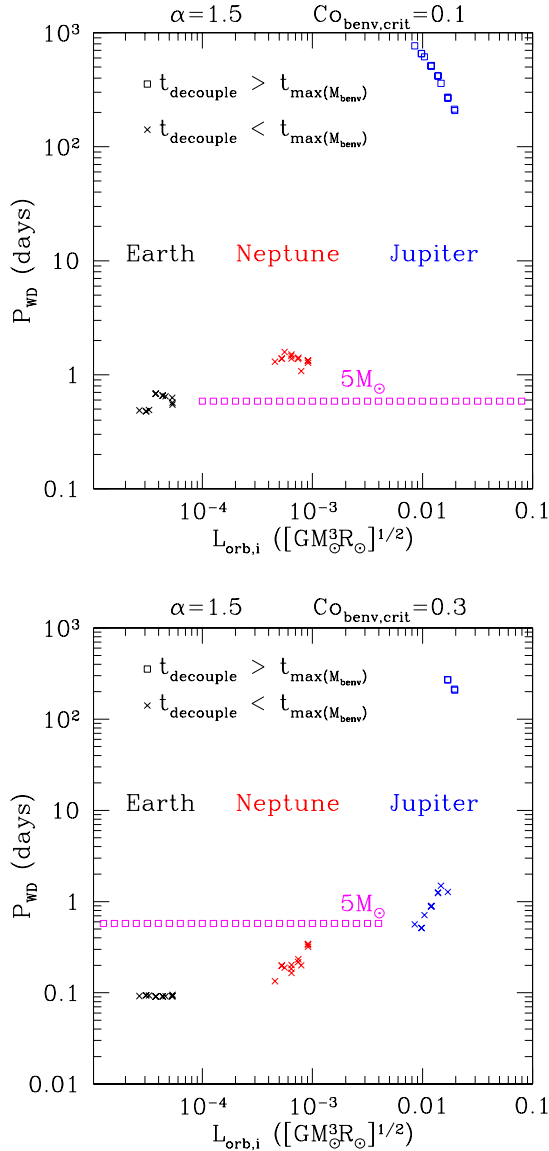


FIG. 13.— Rotation period of $0.55 M_{\odot}$ WD remnant of $1 M_{\odot}$ star, as a function of the initial orbital angular momentum of planetary companion. Squares: Core and envelope remain magnetically coupled until the post-AGB phase. \times 's: Core-envelope decoupling before the final helium shell flash, with J_{wd} set to J_{core} at decoupling. Decoupling takes place when Co_{benv} drops below $\text{Co}_{\text{benv,crit}} = 0.1$ (upper panel) or 0.3 (lower panel). Horizontal magenta line: result for $0.87 M_{\odot}$ remnant of $M_{\text{ZAMS}} = 5 M_{\odot}$ star with 50 km s^{-1} equatorial rotation period.

wind from the surface of the post-AGB star (Figure 12). The spin of the WD remnant is directly proportional to the initial spin period of the star, except in the case of the absorption of a relatively massive ($\gtrsim 3 M_J$) companion. An equatorial rotation speed 50 km s^{-1} on the zero-age MS results in $P_{\text{wd}} \simeq 0.6$ days.

The initial contraction of the envelope also does not cause much of a reduction in J_{core} in the $1 M_{\odot}$ model; but we observe a much stronger decrease following the re-expansion and re-contraction of the envelope that is triggered by a late helium shell instability (Figure 11). This means that the WD remnant of the $5 M_{\odot}$ star has a spin period $P_{\text{wd}} \sim 15$ hr, as compared with ~ 2 yr for

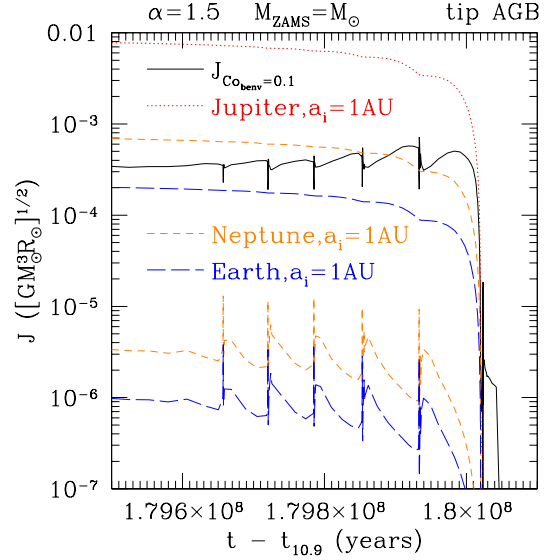


FIG. 14.— Black solid line: minimum J_{\star} that maintains $\text{Co}_{\text{benv}} = 0.1$ near the tip of the AGB of a $M_{\text{ZAMS}} = 1 M_{\odot}$ star. For comparison, colored lines show calculated angular momentum of star absorbing a Jupiter (red dotted), Neptune (orange short-dashed) or Earth (blue long-dashed) starting with $a_i = 1 \text{ AU}$, $e_i = 0$. J_{core} is shown separately for Neptune and Earth interaction, where core and envelope decouple relatively early. Decoupling is delayed to the final super-wind phase when the companion has a Jupiter mass, resulting in lower J_{core} and the longer WD spin seen in Figure 13.

the remnant of the $1 M_{\odot}$ star.

To understand how such a dramatic difference in final WD spin could arise, we consider a simplified analytic model of mass and angular momentum loss from an AGB star. The envelope of the model star has uniform specific angular momentum, the core has a fixed radius R_{benv} , and the core rotates as a solid body with angular velocity $\Omega_{\text{core}} = \Omega_{\text{benv}}$. Mass is lost from the outer boundary of the star, and is also exchanged between core and envelope,

$$\frac{dM_{\text{env}}}{dt} = \frac{dM_{\star}}{dt} - \frac{dM_{\text{benv}}}{dt}. \quad (38)$$

Here M_{env} is the mass of the convective H-rich envelope, and M_{benv} is the mass of (mainly radiative) material inside the base of the envelope. The moment of inertia of the core is initially a small fraction of the total effective moment of inertia

$$I_{\text{eff}} = \frac{J_{\star}}{\Omega_{\text{benv}}} = \frac{2}{3} M_{\text{env}} R_{\text{benv}}^2 + I_{\text{core}}, \quad (39)$$

where we parameterize $I_{\text{core}} = (2\epsilon_{\text{core}}/3) M_{\text{benv}} R_{\text{benv}}^2$.

The coefficient ϵ_{core} is very small, but a key consideration is its relative size compared with the fraction M_{env}/M_{\star} of the stellar mass that is contained in the envelope. We find that ϵ_{core} ranges over $\sim 3 \times 10^{-5} - 10^{-3}$ during the superwind and post-AGB phases. The envelope of the $1 M_{\odot}$ model completes its first contraction while it retains $\sim 10^{-3} M_{\odot}$, but following its re-expansion and re-contraction this mass has dropped to $M_{\text{env}} \sim 10^{-4} M_{\odot}$. In the $5 M_{\odot}$ model, the envelope experiences a single contraction when its mass drops below $\sim 10^{-4} M_{\odot}$. See Figure 15.

Consider first the stage(s) when the envelope is still

inflated, and the core radius R_{benv} changes only slowly. Then

$$\begin{aligned} \frac{dJ_\star}{dt} &= \frac{2}{3} R_\star^2 \Omega(R_\star) \frac{dM_\star}{dt} \\ &= \frac{2}{3} R_{\text{benv}}^2 \Omega_{\text{benv}} \frac{dM_{\text{env}}}{dt} + I_{\text{eff}} \frac{d\Omega_{\text{benv}}}{dt}. \end{aligned} \quad (40)$$

and

$$\frac{1}{\Omega_{\text{benv}}} \frac{d\Omega_{\text{benv}}}{dt} = \frac{dM_{\text{benv}}/dt}{M_{\text{env}} + \epsilon_{\text{core}} M_{\text{benv}}}. \quad (41)$$

Changes in the radius of the star do not enter into these expressions as a result of the uniform specific angular momentum profile in the envelope.

The core mass increases relatively slowly compared with the rapid drop in M_{env} during the peak of the superwind. So Ω_{benv} increases only slightly up to the contraction of the envelope, where it takes the value $\Omega_{\text{benv,col}}$. Beyond that point, the entire star rotates nearly as a solid body. A wind from its surface, which carries away a mass ΔM_\star causes a net spindown

$$\frac{\Omega'_{\text{benv,col}}}{\Omega_{\text{benv,col}}} \simeq \exp \left[-\frac{1}{\epsilon_{\text{core}}} \frac{\Delta M_\star}{M_\star} \right]. \quad (42)$$

This works out to a factor ~ 0.2 decrease in Ω_{benv} in the $1 M_\odot$ model at the onset of the late helium shell flash.

The key step in the dramatic spindown of the post-AGB star involves the re-expansion of the envelope. This occurs by the transfer of $\sim 10^{-3} M_\odot$ of hydrogen-rich material from the radiative part of the star into a rejuvenated convective layer, all occurring at nearly constant total angular momentum. Now the core rotation rate (still equal to the rotation rate at the base of the envelope due to a tight magnetic coupling) decreases to

$$\frac{\Omega_{\text{benv}}}{\Omega'_{\text{benv,col}}} = \frac{\epsilon_{\text{core}} M_{\text{benv}}}{M_{\text{env}} + \epsilon_{\text{core}} M_{\text{benv}}} \sim \frac{\epsilon_{\text{core}} M_{\text{benv}}}{M_{\text{env}}} \sim \frac{1}{30}. \quad (43)$$

(Although the star contracts by a factor ~ 10 in between the initial envelope contraction and the late helium shell flash, ϵ_{core} returns to its pre-contraction value after the re-expansion of the envelope.) The rotation rate of the core remains nearly constant at the value (43), as most of the rejuvenated envelope is expelled.

The net spindown from the initial contraction of the envelope works out to $\Omega_{\text{benv}}/\Omega_{\text{benv,col}} \sim 1/150$. This behavior is neatly encapsulated by the trend of J_\star and J_{core} with the mass $M_\star - M_{\text{wd}}$ remaining to be expelled (Figure 15).

5.3. Minimal Magnetic Flux Enforcing Strong Core-Envelope Coupling

Here we evaluate the minimal magnetic flux that must thread the core-envelope boundary in order for i) the outer radiative core to remain in solid rotation; and ii) the rotation of the inner core to remain coupled to the outer core and inner envelope. A related (although less quantitative) estimate has been made by Spruit & Phinney (1998) for the central cores of massive stars during the later stages of nuclear burning.

First consider the outer core. Although it contains a small fraction of the core mass, it can contribute signifi-

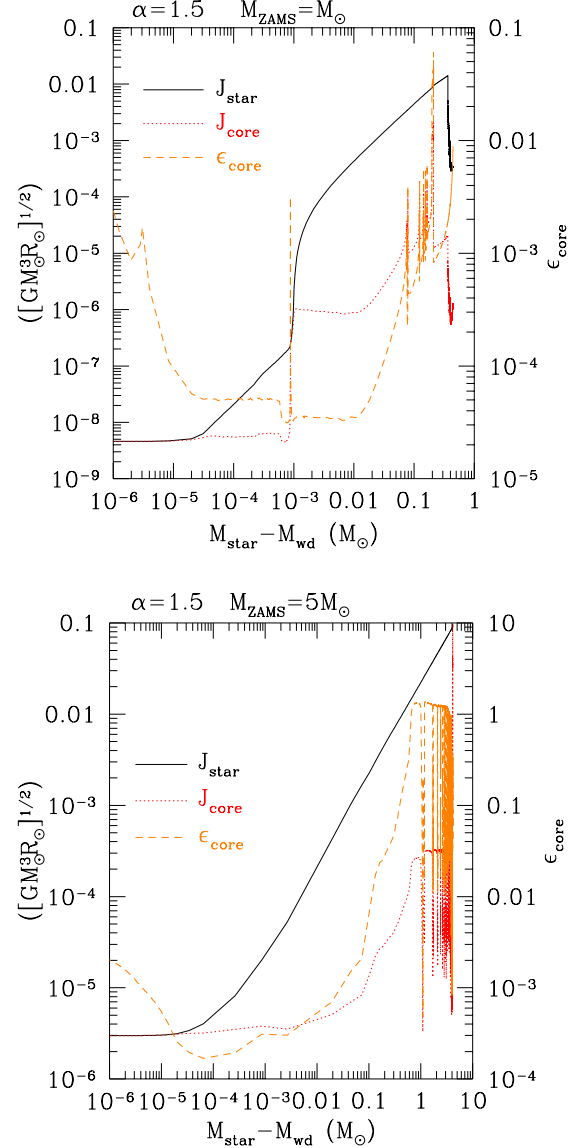


FIG. 15.— Total spin angular momentum of AGB star during the contraction of its hydrogen envelope (black solid line) and the angular momentum of the core (red dotted line). Top panel: $1 M_\odot$ model, including both the initial envelope contraction and the re-expansion following a late helium shell flash. Bottom panel: $5 M_\odot$ model. We show for comparison the dimensionless core moment of inertia $\epsilon_{\text{core}} = I_{\text{core}}/(2/3)M_{\text{benv}}R_{\text{benv}}^2$ (orange short-dash line).

cantly to the moment of inertia. We define a characteristic magnetic flux threading a single hemisphere by setting $B_r/\sqrt{4\pi\rho(R_{\text{benv}})} = |v_r - dR_{\text{benv}}/dt|$:

$$\Phi_{\text{solid}} = \pi R_{\text{benv}}^2 |v_r - dR_{\text{benv}}/dt| \sqrt{4\pi\rho(R_{\text{benv}})}. \quad (44)$$

Next consider changes in the angular momentum of the entire core, which are sensitive to the evolving rotation profile of the envelope. The core angular momentum responds to the applied Maxwell stress $B_r B_\phi/4\pi$ according to

$$I_{\text{core}} \frac{d\Omega_{\text{core}}}{dt} \sim \int \frac{B_r B_\phi}{4\pi} R_{\text{benv}} \sin \theta \cdot 2\pi R_{\text{benv}}^2 \sin \theta d\theta. \quad (45)$$

Taking a second time derivative, making use of the in-

duction equation, we get

$$I_{\text{core}} \frac{d^2 \Omega_{\text{core}}}{dt^2} \sim \frac{1}{2} \int B_r^2 \frac{\partial \Omega}{\partial r} R_{\text{benv}}^4 \sin^3 \theta d\theta. \quad (46)$$

Here the poloidal magnetic field is assumed to be purely radial, so that $\partial_r(r^2 B_r) = 0$, and the integral is evaluated at radius R_{benv} . Integrating over θ then gives

$$I_{\text{core}} \frac{d^2 \Omega_{\text{core}}}{dt^2} \sim \frac{2}{3} B_r^2 R_{\text{benv}}^4 \frac{\partial \Omega}{\partial r}. \quad (47)$$

We take the rotation rate to vary according to

$$\Omega(r, t) \sim \Omega_{\text{benv}} \left(\frac{R_{\text{benv}}}{r} \right)^2 \exp \left[-\frac{t}{\tau_{\Omega}} \right]. \quad (48)$$

Then to avoid spindown on a timescale τ_{Ω} , the magnetic flux must exceed

$$\begin{aligned} \Phi_{\text{couple}} &= \pi R_{\text{benv}}^2 B_r \sim \sqrt{\frac{3}{4}} \pi \frac{I_{\text{core}}^{1/2} R_{\text{benv}}^{1/2}}{\tau_{\Omega}} \\ &\simeq 7.1 \times 10^{20} \text{ Mx} \left(\frac{I_{\text{core}}}{10^{-4} M_{\odot} R_{\odot}^2} \right)^{1/2} \\ &\quad \left(\frac{R_{\text{benv}}}{R_{\odot}} \right)^{1/2} \left(\frac{\tau_{\Omega}}{10^3 \text{ yr}} \right)^{-1}. \end{aligned} \quad (49)$$

We note that τ_{Ω} is controlled by the rate at which material is ejected from the envelope during the final superwind phase, and as a result Φ_{couple} can in principle be larger or smaller than Φ_{solid} (which is determined by the requirement that the core itself remain in solid rotation).

These estimates of the magnetic flux that will enforce a tight rotational coupling between core and envelope are compared in Figures 16 and 17 with the radial flux $(\Delta \mathcal{H})^{1/2}$ that accumulates at the core-envelope boundary. This increment $\Delta \mathcal{H}$ is calculated using Equation (35), taking the timescale for helicity accumulation to be the minimum of the radial drift time $\ell_P/|v_r^{\text{nuc}}|$ and τ_{Ω} .

The larger value of the dynamo-generated flux supports our choice of $\text{Co}_{\text{benv}} < 1$ for core-envelope decoupling. Recall also from Section 3.3 that a tiny poloidal magnetic field – corresponding to $10^{-4} \sqrt{4\pi\rho(R_{\text{benv}})v_{\text{con}}}$ during the later stages of the AGB – will seed a toroidal field in the tachocline that is strong enough to interact buoyantly with the layers above (see Figure 6).

6. MAGNETIC FIELD EMERGENCE AND DECAY

We now consider the emergence of magnetic fields from post-AGB stars, and their subsequent decay. The lifetime of the visible magnetic field at the surface of the star depends on the thickness of the magnetized layer, which in turn depends on the mass of the progenitor and the mass loss rate during the expulsion of the hydrogen envelope.

The strong dredge-up of helium that is experienced by stars of mass $> 2.3 M_{\odot}$ leaves only a thin mass shell to be processed on the AGB. The remainder of the C/O material is generated during core He burning, when the central convective core is decoupled from the exterior and therefore must conserve \mathcal{H} . On the other hand, the helium generated on the RGB is not dredged up in solar-mass stars, and so magnetic fields deposited during both the

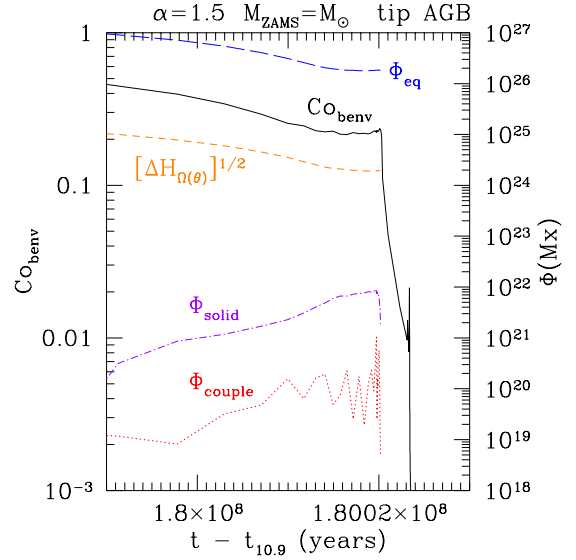


FIG. 16.— Comparison between magnetic flux Φ_{couple} (Equation (49), red dotted line) that maintains core-envelope coupling on the AGB, flux Φ_{solid} (Equation (44), purple dot-dashed line) that maintains solid rotation in the outer core against the inward mass flow, and flux $\Delta \mathcal{H}^{1/2}$ generated by the $\Omega(\theta)$ dynamo process on radial drift time (orange short-dashed line). Blue long-dashed line: magnetic flux corresponding to a poloidal field in equipartition with the convective motions, $\Phi_{\text{eq}} = \pi R_{\text{benv}}^2 \sqrt{4\pi\rho(R_{\text{benv}})v_{\text{con}}^2}$. Solid black line: Coriolis parameter at base of envelope. We argue that the strong dependence of the dynamo-generated field on Co_{benv} allows for core-envelope decoupling below $\text{Co}_{\text{benv}} \sim 0.1 - 0.3$. Fluxes are only plotted up to the final thermal pulse: afterward $dM_{\text{benv}}/dt < 0$ and the coupling of the outer core to the envelope is less sensitive to the instantaneously generated magnetic field.

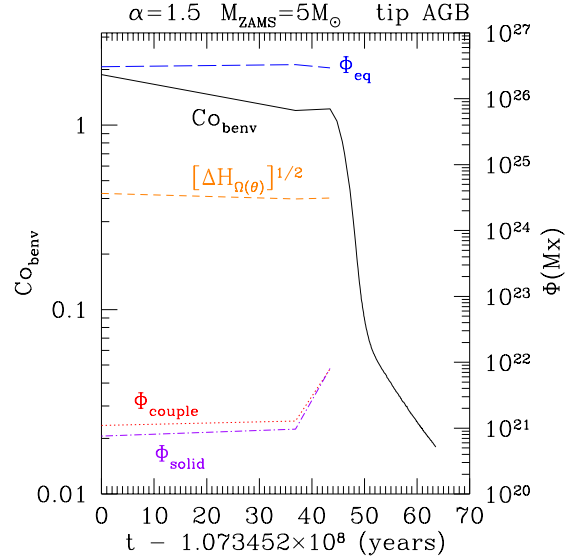


FIG. 17.— Similar to Figure 16, but for the $M_{\text{ZAMS}} = 5 M_{\odot}$ model.

red giant and asymptotic giant phases contribute directly to the remnant WD field.

We found that mass loss on the AGB can push the convective envelope below the threshold for dynamo activity (Figures 11 and 12). In this case, a thin outer layer of the remnant is initially unmagnetized; a strong magnetic field only emerges by ohmic diffusion. We do not consider

any contribution to the magnetic field from the contraction of the final $10^{-4} M_\odot$ of envelope material, which might be rapidly rotating as the result of anisotropic mass loss (Spruit 1998).

The timescale for flux emergence, and the asymptotic decrease in the trapped magnetic flux, are easily obtained from the induction equation,⁴

$$\frac{\partial \mathbf{B}}{\partial t} = -\nabla \times (\eta \nabla \times \mathbf{B}). \quad (50)$$

Here $\eta = c^2/4\pi\sigma$ is the magnetic diffusivity expressed in terms of electrical conductivity σ and speed of light c . For degenerate matter in the liquid state the conductivity can be estimated using (Yakovlev & Urpin 1980; Itoh et al. 1983),

$$\sigma = 8.5 \times 10^{21} \text{s}^{-1} \frac{1}{\Lambda_{ei} \langle Z \rangle} \frac{x^3}{1+x^2}. \quad (51)$$

Here $\Lambda_{ei} \simeq 1$ is the Coulomb logarithm; $\langle Z \rangle = \mu_e \sum X_i Z_i^2 / A_i$, with X_i the mass fraction, Z_i and A_i the nuclear charge and mass of species i , and μ_e is the mean molecular weight per electron. Finally $x = p_F/m_e c$ measures the Fermi momentum of the electrons (of mass m_e). A good approximation to the diffusion timescale through a pressure scale height l_P is

$$t_{\text{diff}, l_P} \simeq \frac{4\pi\sigma l_P^2}{c^2}. \quad (52)$$

An analytic approximation to t_{diff, l_P} is easily obtained in a thin outer shell of mass ΔM that is supported by the pressure of non-relativistic electrons,

$$P = K\rho^{5/3} = \frac{(3\pi^2)^{2/3}}{5} \cdot \frac{\hbar^2}{m_e(\mu_e m_u)^{5/3}} \rho^{5/3}, \quad (53)$$

where

$$P \simeq g \frac{\Delta M}{4\pi R_{\text{wd}}^2} = \frac{GM_{\text{wd}} \Delta M}{4\pi R_{\text{wd}}^4} \quad (54)$$

in a nearly uniform surface gravitational field g . The integration of the equation of hydrostatic equilibrium gives a pressure scale height $l_P = (2/5)(R_{\text{wd}} - r)$ and density $\rho(l_P) = (gl_P/K)^{3/2}$. Substituting σ from equation (51) leads to

$$t_{\text{diff}, \text{analytic}} \sim 1.8 \times 10^{10} \text{ years} \left(\frac{\Delta M}{M_\odot} \right)^{7/5} \left(\frac{M_{\text{wd}}}{M_\odot} \right)^{-3/5} \left(\frac{R_{\text{wd}}}{10^{-2} R_\odot} \right)^{-8/5} \left(\frac{Y_e}{0.5} \right)^2 \left(\frac{\langle Z \rangle}{6} \right)^{-1} \Lambda_{ei}^{-1}. \quad (55)$$

From this expression it is easy to see that the diffusion time through a shell of fixed ΔM depends weakly on the total WD mass.

The diffusion time through the magnetized surface layer of our 0.55 and $0.87 M_\odot$ model WDs is shown in Figures 18 and 19. The longer diffusion time in the $0.55 M_\odot$ remnant is due to the larger magnetized mass.

A direct integration of the induction equation is straightforward if we ignore the continuing hydromagnetic adjustment that must accompany ohmic diffusion.

⁴ Hall drift does not modify an axisymmetric magnetic field in a fluid star, and so we consider only ohmic effects here.

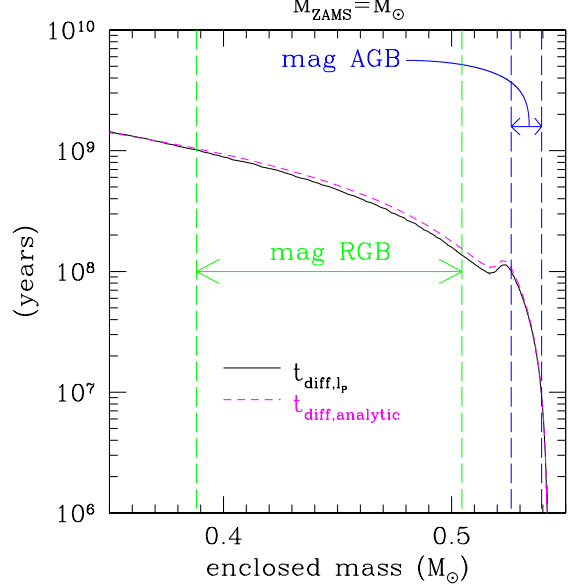


FIG. 18.— Ohmic diffusion time in magnetized layers of $0.55 M_\odot$ WD remnant of $1 M_\odot$ star, as given by Equations (52) (black line) and the analytic fit (55) (magenta dashed line). Mass shells passing through the dynamo-active layer on the RGB (AGB) are bounded by green (blue) dashed lines (when the star has absorbed a Jupiter-mass planet). The hump in the diffusion times close to the surface is caused by a shift in composition and electrical conductivity.

Making the same approximation of a geometrically thin magnetized layer, one has

$$\frac{\partial \Phi_{r,\phi}}{\partial t} = \frac{c^2}{4\pi\sigma(r)} \frac{\partial^2 \Phi_{r,\phi}}{\partial r^2} \quad (56)$$

for both the hemispheric poloidal flux $\Phi_r(r) \simeq 2\pi R_{\text{wd}}^2 \int d(\cos \theta) B_r(r, \theta)$, and the toroidal flux $\Phi_\phi(r, \theta) \simeq 2\pi R_{\text{wd}} \int_r^{R_{\text{wd}}} dr' B_\phi(r', \theta)$ (defined locally in θ).

The decay of the flux is shown in Figure 20, along with the toroidal magnetic energy. We choose a simple initial magnetic configuration with toroidal flux concentrated between depth $0.5\Delta r$ and Δr , where $\Delta r = R_{\text{wd}} - r$ (ΔM is the depth of the magnetized layer. Both the toroidal and poloidal fluxes decrease by a factor $\sim 1/7$ over a time interval 10 times longer than the local decay time $\ell_P^2/\eta(\Delta r)$, as measured at depth Δr .

At the top of the magnetized layer of both model WDs, $t_{\text{diff}, l_P} \sim 10^7$ yr. We conclude that the magnetic field, although initially buried, will emerge at a moderate age in both intermediate-mass and high-mass white dwarfs.

In the $0.55 M_\odot$ remnant of the solar-mass star t_{diff, l_P} extends up to $\sim 1 - 2 \times 10^9$ yr at the base of the magnetized layer; whereas it reaches a maximum $\sim 2 \times 10^8$ yr in the $0.87 M_\odot$ remnant of the $5 M_\odot$ star. Although essentially all WD progeny of intermediate-mass stars will have strong buried toroidal magnetic fields – due to the high angular momentum remaining at the end of the MS – some decay in this buried field is expected at ages exceeding ~ 1 Gyr.

These ohmic timescales depend on the thickness of the C/O layer accumulated on the thermally pulsating AGB. The WD masses we have obtained correspond to a normalization $\eta_B = 0.05$ to the mass-loss rate on the AGB using the formula of Blöcker (1995). There are some

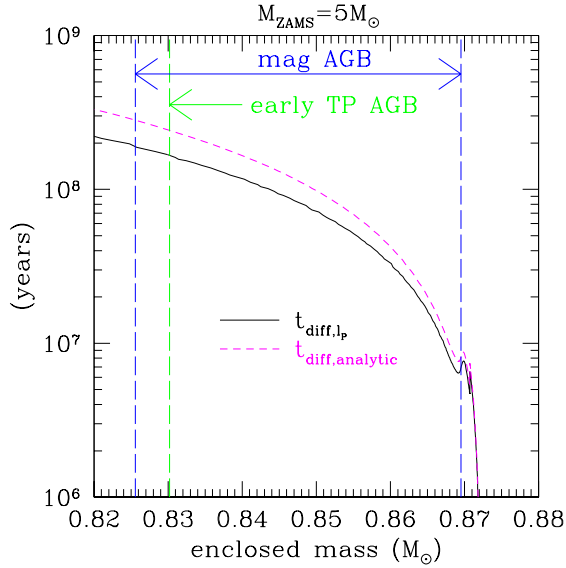


FIG. 19.— Similar to Figure 18, but for $0.87 M_{\odot}$ WD remnant of $5 M_{\odot}$ star. Mass processed during the tail of the first thermal pulse, which produces the majority of the magnetic flux (Figure 8) is bounded by the dashed green line.

suggestions of a lower normalization (e.g. $\eta_B \sim 0.01$, based on the abundance of Li-rich giants in the LMC: Ventura et al. 2000), which implies a larger final C/O core. For example, increasing the remnant mass of the $5 M_{\odot}$ progenitor to $\sim 0.90 M_{\odot}$ results in an ohmic diffusion time $\sim 4 \times 10^8$ yr at the base of the magnetized layer). One sees from Figure 20 that any toroidal flux buried in such a WD will have decreased by a factor $\sim 1/5$ from its post-AGB value by an age 3×10^9 yr.

Whether this decay of a buried field corresponds to significant decay of the surface dipole magnetic field – or even to growth – remains uncertain because the two components do not evolve independently. Ohmic diffusion of the magnetic field is so slow that the magnetic field easily makes a continuing hydromagnetic adjustment to something close to magnetostatic equilibrium. An interchange between the toroidal and poloidal components is possible without any change in \mathcal{H} .

7. SUMMARY AND COMPARISON WITH ALTERNATIVE THEORETICAL APPROACHES

We have investigated how the rotation and magnetism of a giant star respond to the inward advection of a small amount of angular momentum by deep convective plumes in the extended envelope. Some features of the dynamo process operating near the core-envelope boundary are unique to giants: namely those driven by the intense radiation flux and the rapid inward drift of material to the burning shell(s). The buoyancy that is induced by radiative heating of magnetized material strongly enhances the rate of mixing between core and envelope.

Even a weak helical magnetic field enforces a rotational coupling between core and envelope, and maintains nearly solid rotation in the core. The inflow of mass into the core is accompanied by an inflow of magnetic helicity, which is needed to sustain a stable, large-scale magnetic field in the white dwarf remnant. The compensating helicity is lost through the surface of the star.

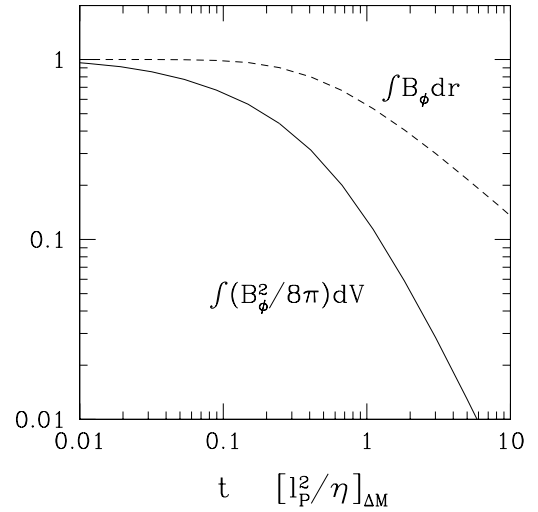
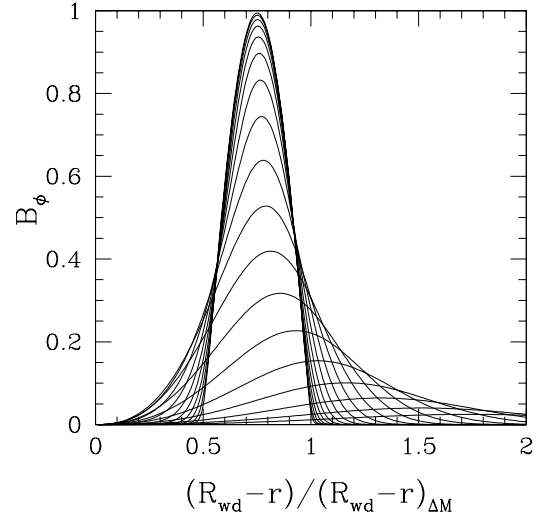


FIG. 20.— Top panel: ohmic diffusion of toroidal magnetic field initially concentrated at depths $0.5\Delta r$ to $\Delta r \ll R_{wd}$ below the surface of a cold white dwarf. Here Δr is the maximum depth of the magnetized layer of mass ΔM . Bottom panel: decrease of the toroidal (or radial) magnetic flux threading this layer, along with the toroidal magnetic energy, both normalized to the initial values. This calculation does not allow for an interchange between toroidal and poloidal fluxes resulting from a hydromagnetic instability that might accompany ohmic drift.

This strong core-envelope coupling is easily maintained in subgiants and core He burning stars, as we found in Paper I. It is also sustained near the tips of the RGB and AGB in isolated intermediate-mass stars if angular momentum is distributed broadly within the slowly rotating parts of the envelope. We found that the threshold for dynamo action is easily reached when $\Omega \propto r^{-2}$ at $\text{Co} \lesssim 1$.

Injection of angular momentum from a planetary or stellar companion is needed to maintain a magnetic core-envelope coupling during the giant expansion of late-type stars that lose most of their initial spin to magnetized winds (corresponding to $M_{ZAMS} \lesssim 1.3 M_{\odot}$).

Although a strong coupling does not depend on angular momentum injection in intermediate-mass stars, the remnant magnetic field may be significantly enhanced by

the absorption of a massive planet or brown dwarf, due to the relatively low mass of the outer shell that becomes magnetized.

These results are broadly consistent with an increased incidence of strong magnetism in i) massive WDs, and ii) accreting WDs in CVs, which experienced a tidal interaction before and during a common-envelope phase.

The strength of the remnant dipole magnetic field is directly tied to the magnetic helicity that has accumulated in the hydrogen-depleted core. Helicity growth depends on a combination of i) efficient angular momentum transport by poloidal magnetic fields through the outer core; and ii) a persistent radial angular velocity gradient in the tachocline that is driven by angular inhomogeneities in the rotation rate in the surrounding convective envelope. The helicity flux is roughly proportional to the rotational kinetic energy of the inner envelope.

The WD dipole fields so obtained can exceed 10^7 G in both the $0.55 M_\odot$ WD remnant of a solar-mass star that absorbs a Jupiter, and the $0.87 M_\odot$ remnant of a $5 M_\odot$ star that has no binary interaction (Figure 9). In the former case, the engulfment of companion much more massive than Jupiter requires exceptional circumstances, and this field can be considered a approximate upper limit. In the latter case, the engulfment of much more massive companion, even $\sim 0.1 M_\odot$, may be significantly more common. This results in an increased remnant field, reaching as high as $\sim 10^8$ G (Figure 10).

These field strengths do not approach the strongest measured in WDs ($\sim 10^9$ G), which however are very rare. The strongest fields may therefore originate in more extreme merger events such as the collision of two WDs (e.g. García-Berro et al. 2012).

The engulfment of an Earth-mass planet by an evolved solar-mass star, which barely augments the angular momentum of the star, results in a WD dipole field of $\sim 10^6$ G. In this case, we find that most of the magnetic helicity is deposited during a brief interval at the start of core He burning. The star falls below the threshold for dynamo activity near the tips of the RGB and AGB. Even a mild enhancement of wind-driven angular momentum loss, or a softening of the rotation profile in the envelope, would eliminate most of this MG magnetic field.

The magnetic field generated on the giant branches is initially buried in the WD (in cases where AGB core and envelope decouple before the final thermal pulse) but diffuses ohmically outward over the first $\sim 10^7$ yr. A strong internal toroidal field begins to decay at an age $\sim 4 \times 10^8$ yr in a $\sim 0.9 M_\odot$ WD, as compared with $\sim 2 \times 10^9$ yr in a $0.55 M_\odot$ WD. We find that the net decay is by a factor ~ 0.2 at an age $\sim 3 \times 10^9$ yr in a $0.9 M_\odot$ WD. The initial decay of the toroidal field may be accompanied by transient growth of the external dipole, which is possible at constant internal magnetic helicity. On the observational side, the compilation of magnetic WDs in Kepler et al. (2013) only extends to an age ~ 1 Gyr, and the incidence of magnetism in older WDs remains uncertain.

We find that the spin angular momentum of the remnant WD of a late-type star can, in some circumstances, *anti-correlate* with the angular momentum of the star during the AGB phase. In stars that retain only a moderate angular momentum at the end of the AGB (less

than the orbital angular momentum of Jupiter), this decoupling sets in before the final helium shell flash. The final WD spin then depends most directly on the critical Coriolis parameter below which the envelope dynamo fades away in the inner envelope. In the case of absorption of a Neptune-mass planet during the post-MS evolution of a $1 M_\odot$ star, P_{wd} lies between 0.1 and 1 d. This residual spin rate is a lower bound, as it does not include a contribution from a final anisotropic contraction of the envelope (Spruit 1998).

The situation changes if the star is massive enough to retain most of its natal angular momentum, or if it absorbs a Jupiter-mass planet or brown dwarf. Then core and envelope should remain coupled beyond the final helium shell flash, and spindown of the core can be directly related to a transient reduction in core mass. The angular momentum that is retained by the core during the contraction of the envelope depends on whether the core experiences a late re-expansion due to a delayed helium shell instability. A transfer of mass $M_{\text{env}} \gg \epsilon_{\text{core}} M_\star$ to the envelope, combined with ejection of most of this envelope material, implies strong spindown of the core. The net result is that the final WD spin period can exceed a year in our $1 M_\odot$ model. This final spindown was found to be significantly smaller in the $5 M_\odot$ model, resulting in P_{wd} shorter than a day, because of the smoother transition to the post-AGB phase.

7.1. Some Outstanding Issues

Sensitivity to strength of angular-momentum pumping in giant envelope. The Kepler asteroseismological data give a calibration of the envelope rotation profile in subgiants – as investigated in detail in Paper I – but not in stars larger than $\sim 10 R_\odot$. Here we have considered the consequences of uniform dJ/dM in the slowly rotating parts of the envelope. This zone with $\text{Co} < 1$ extends deep into the star near the tips of the RGB and AGB, unless the star interacts with a relatively massive binary companion. A rotation profile $\Omega \propto r^{-2}$ in the outer envelope is supported by the numerical simulations of Brun & Palacios (2009).

The orbital angular momentum of a Jupiter can be compared with the minimum rotational angular momentum that will sustain a dynamo near the tip of the AGB. Starting the planet at $a_i = 1$ AU, the excess is about a factor $\sim 30(\text{Co}_{\text{benv,crit}}/0.3)^{-1}$ in our $1 M_\odot$ model. The shallowest rotation profile which could maintain a minimal Coriolis parameter $\text{Co}_{\text{benv}} \sim 0.3$ in an envelope of depth $R_{\text{benv}}/R_\star \sim 0.01$ is $\Omega(r) \propto r^{-4/3}$. In this situation, the amplitude of the helicity flux into the core, which is proportional to Ω_{benv}^2 (Equation (35)), would be reduced by a factor $\sim 10^{-3}$. The corresponding reduction in B_{dipole} , by a factor ~ 0.03 , would still allow for fields of order MG (see Figure 9), but not magnetic fields $\gtrsim 10$ MG.

A related consideration is the steepness of the angular velocity profile in the inner envelope, where $\text{Co} \gtrsim 1$, and its effect on the upper range that is obtained for the WD magnetic field. In this paper we did not simply take the profile that was determined in Paper I from asteroseismic models of sub-giant and helium burning stars. During these relatively compact evolutionary phases, an inner rotation profile $\Omega(r) \propto r^{-1}$ corresponds to $\text{Co}_{\text{benv}} \sim 10$

30. This profile is consistent with the inward pumping of angular momentum by deep convective plumes in an adiabatic envelope with gravity $g(r) \propto r^{-1}$. A lower inner Coriolis parameter would be maintained near the tips of the RGB and AGB if the same rotation profile were sustained there.

In fact, the rotation profile is expected to steepen to $\Omega(r) \sim r^{-3/2}$ in the presence of a similar convective structure, due to the contraction of the core and the steepening of the gravity profile. For this reason, we allow the inner index in Equation (4) to increase to $\alpha = 3/2$ during the expanded phase where magnetic helicity growth is concentrated, and the remnant WD spin angular momentum is determined. The net effect is to raise the upper envelope of the magnetic field distribution in massive WDs from ~ 3 MG ($\alpha = 1$) to 10-30 MG ($\alpha = 3/2$). The limiting magnetization and spins of lower-mass WDs hardly change over this range of α .

What happens to any core magnetic field left over from the MS phase, when exposed to the turbulent motions in a slowly rotating convective envelope ($\text{Co}_{\text{benv}} \ll 1$)? Consider taking the magnetic flux threading a WD and spreading it across the core-envelope boundary of the progenitor during its AGB expansion. Even a MG magnetic field in the WD becomes dynamically insignificant, $B_r(R_{\text{benv}}) \sim 10^{-4}(4\pi\rho v_{\text{con}}^2)^{1/2}$. Such a weak poloidal magnetic field would rapidly diffuse over the boundary sphere, causing fluid elements that are threaded by radial field of opposing signs to be mixed together. In this situation it is difficult to see how the material flow from the envelope into the core could maintain a large-scale poloidal magnetic field unless it were self-consistently maintained by a dynamo process. A numerical experiment studying the diffusion and reconnection of such a seed field across the spherical boundary between radiative and convective layers is feasible and would provide interesting results.

Relaxation of helical magnetic field to the ‘maximum-dipole’ configuration. The surface dipole magnetic of the WD remnant has been estimated assuming that $\Phi_r \sim \Phi_\phi \sim \mathcal{H}^{1/2}$. Other magnetic configurations are possible, especially those with relatively stronger toroidal fields, corresponding to $\Phi_\phi \gg \Phi_r = (\mathcal{H}/\Phi_\phi)^{1/2}$ (Braithwaite 2009). Ohmic diffusion in WD stars with strong toroidal fields may cause some transient growth of the dipole field, as the magnetic field relaxes to a more isotropic configuration.

Dispersion in magnetic field strength in massive WDs. Although a greater fraction of massive WDs exhibit strong magnetic fields than do their $\sim 0.55 - 0.6 M_\odot$ cousins, a majority do not. Intermediate-mass stars retain more angular momentum at the end of the MS, thereby facilitating a dynamo. This angular momentum can, nonetheless, be enhanced by the absorption of a massive planet, brown dwarf, or low-mass star, or a tidal interaction with a stellar companion. Other effects causing dispersion in the visible surface magnetic field include exchange between toroidal and poloidal magnetic fluxes, and the time spent by the progenitor star during the thermally pulsating AGB phase.

Emergence of ‘frozen’ magnetic field generated during the pre-MS phase (or during MS core convection)? The outer $0.3 M_\odot$ of the $0.55 M_\odot$ WD is processed through

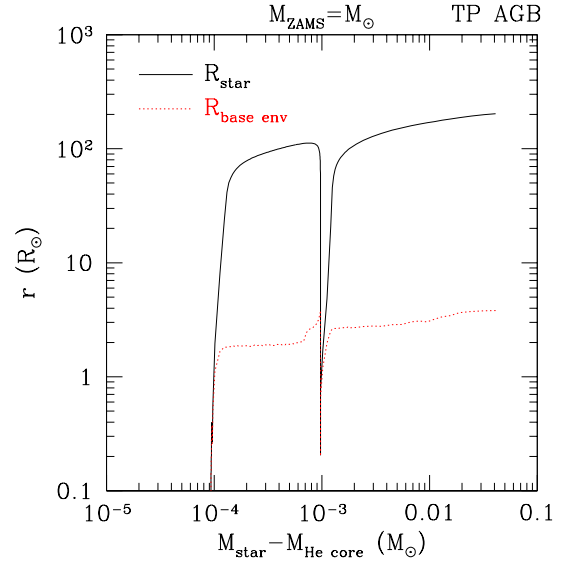


FIG. 21.— Dependence of AGB stellar radius R_* (black line) and base of convective envelope R_{benv} (dotted red line) on residual H mass. Endpoint of $M_{\text{ZAMS}} = 1 M_\odot$ model.

a deep convective envelope during the RGB and AGB phases. The proportion of this material which experiences rapidly rotating convection, and develops a strong magnetic field, depends on the initial placement of planets around the star. For example, if the closest Neptune or Jupiter orbits at a distance ~ 1 AU, then only the outer half of the processed layer is strongly magnetized.

The ohmic diffusion time from the base of this processed layer approaches a Hubble time, independent of the architecture of the planetary system. From this we conclude that the magnetization of all but the very oldest ~ 0.55 - $0.6 M_\odot$ WDs is not significantly influenced by a ‘frozen’ core magnetic field.

The assembly history is very different for the massive WD remnants of intermediate-mass stars. Now the bulk of the WD mass is processed during core H and He burning, which leave unaltered the magnetic helicity stored in the stellar core. In the case of an isolated $\sim 0.9 M_\odot$ WD, a core magnetic field could emerge ohmically through the outer $\sim 0.05 - 0.1 M_\odot$ that is processed on the thermally pulsating AGB, but only with a delay of $\sim 2 - 5 \times 10^8$ yr (depending on the normalization of mass loss during this phase). A growth in the incidence of magnetism in older WDs could therefore point to a contribution of such a ‘frozen’ field to the visible surface field. (But not exclusively so, given the competing possibility of dipole field growth mediated by the decay of a toroidal field that is buried in a thin outer mass shell.)

Implications of Binary Magnetic WDs. The incidence of strong magnetism (exceeding 10^7 G and implying classification as a ‘polar’) exceeds $\sim 30\%$ in short-period CVs with ages exceeding ~ 1 Gyr (Gänsicke 2005). Our calculations suggest that these fields might decay significantly in more massive isolated WDs. Long-lived magnetism in old binary WDs with periods < 2 hr (below the ‘period gap’) could be maintained by the accretion of $\gtrsim 0.1 M_\odot$ from the companion, which would have the effect of pushing down the magnetized layers to a greater depth and a longer ohmic timescale.

7.2. Competing effects of a collapsing low-mass ($\sim 10^{-4} M_\odot$) AGB envelope

The final contraction of an AGB envelope, beginning at a photospheric radius $\sim 10^2 R_\odot$, leaves behind a hydrogen layer of mass $M_{\text{env},f} \sim 10^{-4} M_\odot$. Mass loss slows down significantly as the star contracts inside a radius $R_{\text{pAGB}} \sim R_\odot$ (Figure 21).

It is possible that the process driving mass loss is so anisotropic that the collapsing envelope carries with it a significant angular momentum, equal and opposite to that lost during the final stages of the super-wind (Spruit 1998). An upper bound to the angular momentum thus added to the post-AGB star can be obtained as follows. The collapsed envelope will experience a bar instability and spread outward into a disk if its angular velocity exceeds $\sim 0.3(GM_{\text{wd}}/R_{\text{pAGB}}^3)^{1/2}$ at radius R_{pAGB} . Any angular momentum in excess of $J_{\text{max}} \sim 0.3M_{\text{env},f}(GM_{\text{wd}}R_{\text{pAGB}})^{1/2}$ is transported outward by viscous torques in the disk, and is presumably lost in a wind.

Setting the envelope angular momentum to this limiting value, and assuming that it is shared with the rest of the star at radius R_{pAGB} , we obtain a minimum spin period for the cold WD remnant,

$$P_{\text{wd}} \geq \frac{2\pi I_{\text{wd}}}{J_{\text{max}}} = 0.4 \left(\frac{M_{\text{env},f}}{10^{-4} M_\odot} \right)^{-1} \left(\frac{R_{\text{pAGB}}}{R_\odot} \right)^{-1/2} \text{ hr.} \quad (57)$$

A comparison with Figure 13 shows that somewhat faster WD spins can be imparted by rotating envelope contraction than would result from a cutoff of the envelope dynamo before the final intense phase of mass loss. However, the fastest WD spins may depend on a merger between two WDs.

7.3. Impulsive Dynamo Amplification in a Merger?

The formation of magnetic WDs in stellar binaries is considered by Tout et al. (2008). It is noted that the injection of angular momentum from a binary companion (either a low-mass MS star or a substellar companion) into a giant star will trigger strong differential rotation in its core and envelope. This differential rotation may spark the impulsive growth of the magnetic field in the core, further details of which have been examined by Wickramasinghe et al. (2014).

Nordhaus et al. (2011) consider the tidal shredding of a planetary companion close to the giant core. They argue that this material initially forms a disk in nearly Keplerian rotation about the core, in which a magnetic field is generated by the magnetorotational instability. The most promising application of this process is to isolated magnetic WDs, since it may be difficult for a planet and a stellar companion (later the mass donor in a CV system) to co-exist on similar orbits.

The contribution made by such an impulsive dynamo to the net magnetic helicity stored in the stellar core can be compared with the longer term effect examined in this paper. When the companion is tidally disrupted (either within the convective envelope, or within the rarefied mantle surrounding the burning shells), the mass M_2 deposited would be re-distributed back through the

convective envelope on the thermal timescale

$$t_{\text{th}} \sim \frac{GM_{\text{core}}M_2}{R_{\text{tide}}L_{\text{AGB}}} \sim 600 \left(\frac{M_2}{0.1 M_\odot} \right) \left(\frac{R_{\text{tide}}}{R_\odot} \right) \text{ yr.} \quad (58)$$

As envisaged by Nordhaus et al. (2011), a centrifugally supported disk may spread on a shorter timescale than (58), in which case the internal heat generated in the disk is advected around without being radiated back into the surrounding stellar envelope. Studies of advective accretion flows in other contexts (e.g. Blandford & Begelman 1999) suggest that a fraction of the disk material would be accreted deeper into the gravitational potential of the degenerate core, which may be enough to transiently increase its rotation.

Since the energy released by H burning easily suffices to unbind the ashes from the degenerate core, any such rapidly accreted material must remain H rich. On the longer thermal timescale, this nuclear energy can be radiated away, accompanied by a relaxation of the outer core to its equilibrium structure. The mass δM_{nuc} processed by H and He burning during that relaxation is small compared with the total deposited mass M_2 . Given that a mass M_{acc} is accreted close to the burning radius $R_{\text{burn}} \sim 0.1 R_\odot$, one has

$$\begin{aligned} \delta M_{\text{nuc}} &\sim \frac{GM_{\text{core}}}{\varepsilon_{\text{nuc}}R_{\text{burn}}} M_{\text{acc}} \\ &\sim 2 \times 10^{-3} \left(\frac{R_{\text{burn}}}{0.1 R_\odot} \right)^{-1} \left(\frac{M_{\text{acc}}}{M_2} \right) M_2. \end{aligned} \quad (59)$$

The normalization is about ~ 10 times larger if H burning is extinguished, so that only the He-burning shell remains active.

We see that a relatively small mass is incorporated into the C/O core before the star adjusts to a new equilibrium structure. Given that the magnetic coupling between core and envelope is sustained, most of the added angular momentum in this new equilibrium state will be stored in the outer envelope.

The large-scale Maxwell stress $B_r B_\phi / 4\pi$ in the outer core may easily increase by a factor $\sim 10^4$ in the immediate aftermath of the tidal disruption, when the rotation frequency increases by $\gtrsim 10^2$. However, as the envelope dredges up the injected angular momentum, we expect the Maxwell stress to adiabatically adjust downward, since little mass flows into the core. Such a downward adjustment could be avoided if the magnetic field lines became decoupled from the envelope, but that does not seem consistent with the rapid buoyant motion of such a strong magnetic field (see Equation (19)).

From this perspective, the *impulsive* growth of the magnetic field following the tidal disruption of a low-mass star or substellar companion may leave little permanent mark on the magnetization of the C/O core. A merger during the early post-MS expansion could induce some direct hydrodynamic mixing with the hydrogen-depleted core, but only when the accumulated helium mass was still well below the final WD mass.

We argue that the dominant effect of such a merger is, instead, to i) push the envelope above the threshold for a gentler and more persistent dynamo process in low-mass giant stars, $M_{\text{ZAMS}} \lesssim 1.3 M_\odot$; and ii) to augment the inward flux of magnetic helicity in stars which remain

rapidly rotating at the end of the MS.

The merger of two WDs (or of a WD with the core of an evolved companion) provides the main counter-example to these conclusions. Now hydrogen-depleted material in the more massive WD experiences direct hydrodynamic mixing with the tidally shredded remnants of the companion. The rate of such events appears to be

relatively small, and may therefore only accomodate the most strongly magnetized WDs.

We would like to thank David Arnett and Peter Goldreich for conversations. This work was supported by NSERC.

APPENDIX

TWISTING OF A RADIAL MAGNETIC FIELD

Here we construct expressions describing the large-scale flow of magnetic helicity in the evolving core of a giant star. The rotation profile and magnetic field are assumed to be axisymmetric, but departures from reflection symmetry about the rotation axis are considered.

Our treatment is simplified by considering a weak radial magnetic field with angular flux profile

$$\Phi_r(\theta) = \int_0^\theta \sin \theta' r^2 B_r(\theta') d\theta' \quad (\text{A1})$$

and corresponding potential

$$A_\phi(\theta, r) = \frac{1}{r \sin \theta} \Phi_r(\theta). \quad (\text{A2})$$

In what follows, we therefore neglect any radial change in $\Phi_r(\theta)$.

A dynamo operating near the convective boundary will generally supply a poloidal field of a fluctuating sign, but the contribution to $\mathbf{A} \cdot \mathbf{B}$ in one hemisphere is insensitive to this sign. The contributions from the two hemispheres generally have opposing signs.

Consider the case where the rotation profile is reflection-symmetric, so that convective motions enforce a certain $\partial\Omega/\partial r$ at polar angles θ and $\pi - \theta$. The evolution of the twist in the core depends on the connectivity of the poloidal magnetic field. If both angles θ and $\pi - \theta$ are connected by the same (axially-symmetric) magnetic flux surface, then there is no evolution of the net twist along this flux surface. On the other hand, if the distribution of magnetic flux is different across the two hemispheres, then a given flux surface will experience a net differential winding.

The rate of change of \mathcal{H} inside a spherical boundary of a fixed radius r is

$$\frac{\partial \mathcal{H}}{\partial t} = - \int dS \hat{r} \cdot [c\phi \mathbf{B} + (\mathbf{A} \cdot \mathbf{B})\mathbf{v} - (\mathbf{A} \cdot \mathbf{v})\mathbf{B}], \quad (\text{A3})$$

where the bounding sphere is placed just inside the convective boundary.

The electrostatic potential ϕ appearing on the right-hand side of (A3) is driven by the mean rotation of the star. The corresponding electric field $\mathbf{E} = -(\boldsymbol{\Omega} \times \mathbf{r}) \times \mathbf{B}/c$ is sourced by

$$\phi(\theta, r) = \frac{1}{c} \Omega(r) \Phi_r(\theta). \quad (\text{A4})$$

Differential rotation generates A_r (and thence helicity) via

$$\frac{\partial A_r}{\partial t} = -\frac{\partial \Omega}{\partial r} \Phi_r(\theta). \quad (\text{A5})$$

The electrostatic potential cancels off the term $A_\phi \hat{\phi} \cdot (\boldsymbol{\Omega} \times \mathbf{r})$ in Equation (A3), and we are left with

$$\frac{d\mathcal{H}}{dt} = \frac{\partial \mathcal{H}}{\partial t} + \frac{dR_{\text{benv}}}{dt} \int dS A_\phi B_\phi = -\delta v_r \int dS A_\phi B_\phi. \quad (\text{A6})$$

Here we have subtracted off the velocity of the convective boundary from the radial flow speed v_r of spherical mass shells:

$$\delta \mathbf{v} = \mathbf{v} - \frac{dR_{\text{benv}}}{dt} \hat{r}. \quad (\text{A7})$$

On the AGB, v_r is negative and larger in magnitude than dR_{benv}/dt , but we include this correction for completeness.

Because the poloidal flux surfaces are, in this treatment, fixed in position, it is useful to re-express the toroidal field in terms of a twist angle ϕ_B :

$$B_\phi(r, \theta) = \frac{\partial \phi_B}{\partial r} r \sin \theta B_r. \quad (\text{A8})$$

The toroidal component of the induction equation is

$$\frac{\partial B_\phi}{\partial t} = B_r r \sin \theta \frac{\partial \Omega}{\partial r} - \frac{1}{r} \frac{\partial}{\partial r} (r B_\phi v_r), \quad (\text{A9})$$

which simplifies to

$$\frac{d}{dt} \left(\frac{\partial \phi_B}{\partial r} \right) = \frac{\partial^2 \phi_B}{\partial t \partial r} + v_r \frac{\partial^2 \phi_B}{\partial r^2} = \frac{\partial \Omega}{\partial r} - \frac{\partial v_r}{\partial r} \frac{\partial \phi_B}{\partial r}. \quad (\text{A10})$$

in the case (considered here) that Φ_r only depends on latitude.

Substituting expression (A8) into (A6) gives

$$\frac{d\mathcal{H}}{dt} = -2\pi\delta v_r \int d\theta \Phi_r \frac{\partial \Phi_r}{\partial \theta} \frac{\partial \phi_B}{\partial r}, \quad (\text{A11})$$

which mirrors the standard expression for a static plasma.

In general the radial magnetic flux profile differs in shape, as well as sign, between the two hemispheres. A complete cancellation in the integral over θ in Equation (A11) remains possible if ϕ_B is independent of θ . That would be the case if fluid stresses were to smooth out latitudinal differential rotation within each shell, so that $\partial\Omega/\partial r$, the source for ϕ_B , were only a function of radius. We see that a net flux of magnetic helicity into the core depends on *latitudinal* differential rotation – differential rotation across flux surfaces – which is a generic consequence of convection.

REFERENCES

- Angel, J. R. P., Borra, E. F., & Landstreet, J. D. 1981, *ApJS*, 45, 457
- Aurière, M., Donati, J.-F., Konstantinova-Antova, R., et al. 2010, *A&A*, 516, LL2
- Aurière, M., Konstantinova-Antova, R., Charbonnel, C., et al. 2014, *A&A*, 574, A90, submitted (arXiv:1411.6230v1)
- Balbus, S. A. & Hawley, J. F. 1994, *MNRAS*, 266, 769
- Beck, P. G., Montalbán, J., Kallinger, T., De Ridder, J., Aerts, C., García, R. A., Hekker, S., Dupret, M.-A., Mosser, B., Eggenberger, P., Stello, D., Elsworth, Y., Frandsen, S., Carrier, F., Hillen, M., Gruberbauer, M., Christensen-Dalsgaard, J., Miglio, A., Valentini, M., Bedding, T. R., Kjeldsen, H., Girouard, F. R., Hall, J. R., & Ibrahim, K. A. 2012, *Nature*, 481, 55
- Bildsten, L., Paxton, B., Moore, K., & Macias, P. J. 2012, *ApJ*, 744, LL6
- Blackman, E. G., & Field, G. B. 2000a, *ApJ*, 534, 984
- Blackman, E. G., & Field, G. B. 2000b, *MNRAS*, 318, 724
- Blackman, E. G., Frank, A., Markiel, J. A., Thomas, J. H., & Van Horn, H. M. 2001, *Nature*, 409, 485
- Blackman, E. G., & Thomas, J. H. 2015, *MNRAS*, 446, L51
- Blandford, R. D., & Begelman, M. C. 1999, *MNRAS*, 303, L1
- Blöcker, T. 1995, *A&A*, 297, 727
- Braithwaite, J. 2009, *MNRAS*, 397, 763
- Braithwaite, J. & Spruit, H. C. 2004, *Nature*, 431, 819
- Brun, A. S. & Palacios, A. 2009, *ApJ*, 702, 1078
- Cantiello, M., Mankovich, C., Bildsten, L., Christensen-Dalsgaard, J., & Paxton, B. 2014, *ApJ*, 788, 93
- Charbonneau, P. 2014, *ARA&A*, 52, 251
- Cline, K. S., Brummell, N. H., & Cattaneo, F. 2003, *ApJ*, 599, 1449
- Dobbie, P. D., Napiwotzki, R., Burleigh, M. R., Williams, K. A., Sharp, R., Barstow, M. A., Casewell, S. L., & Hubeny, I. 2009, *MNRAS*, 395, 2248
- Dorch, S. B. F. 2004, *A&A*, 423, 1101
- Ferrario, L. & Wickramasinghe, D. T. 2005, *MNRAS*, 356, 615
- Gänsicke, B. T. 2005, in *Astronomical Society of the Pacific Conference Series*, Vol. 330, *The Astrophysics of Cataclysmic Variables and Related Objects*, ed. J.-M. Hameury & J.-P. Lasota, 3, (San Francisco: Astron. Soc. of the Pacific)
- García-Berro, E., Lorén-Aguilar, P., Aznar-Siguán, G., et al. 2012, *ApJ*, 749, 25
- Gough, D. O. & McIntyre, M. E. 1998, *Nature*, 394, 755
- Gruzinov, A. V., & Diamond, P. H. 1994, *Physical Review Letters*, 72, 1651
- Itoh, N., Mitake, S., Iyetomi, H., & Ichimaru, S. 1983, *ApJ*, 273, 774
- Kepler, S. O., Pelisoli, I., Jordan, S., Kleinman, S. J., Koester, D., Külebi, B., Peçanha, V., Castanheira, B. G., Nitta, A., Costa, J. E. S., Winget, D. E., Kanaan, A., & Fraga, L. 2013, *MNRAS*, 429, 2934
- Kissin, Y., & Thompson, C. 2015, *ApJ*, 808, 35
- Liebert, J., Bergeron, P., & Holberg, J. B. 2003, *AJ*, 125, 348
- Liebert, J., Wickramasinghe, D. T., Schmidt, G. D., Silvestri, N. M., Hawley, S. L., Szkody, P., Ferrario, L., Webbink, R. F., Oswalt, T. D., Smith, J. A., & Lemagie, M. P. 2005, *AJ*, 129, 2376
- Livio, M., & Soker, N. 2002, *ApJ*, 571, L161
- Menou, K., Balbus, S. A., & Spruit, H. C. 2004, *ApJ*, 607, 564
- Moss, D., Tuominen, I., & Brandenburg, A. 1991, *A&A*, 245, 129
- Mosser, B., Goupil, M. J., Belkacem, K., Marques, J. P., Beck, P. G., Bloemen, S., De Ridder, J., Barban, C., Deheuvels, S., Elsworth, Y., Hekker, S., Kallinger, T., Ouazzani, R. M., Pinsonneault, M., Samadi, R., Stello, D., García, R. A., Klaus, T. C., Li, J., Mathur, S., & Morris, R. L. 2012, *A&A*, 548, A10
- Nordhaus, J., Blackman, E. G., & Frank, A. 2007, *MNRAS*, 376, 599
- Nordhaus, J., Busso, M., Wasserburg, G. J., Blackman, E. G., & Palmerini, S. 2008, *ApJ*, 684, L29
- Nordhaus, J., Wellons, S., Spiegel, D. S., Metzger, B. D., & Blackman, E. G. 2011, *Proceedings of the National Academy of Science*, 108, 3135
- Parker, E. N. 1993, *ApJ*, 408, 707
- Paxton, B., Bildsten, L., Dotter, A., Herwig, F., Lesaffre, P., & Timmes, F. 2011, *ApJS*, 192, 3
- Reiners, A., Basri, G., & Browning, M. 2009, *ApJ*, 692, 538
- Ruderman, M. A. & Sutherland, P. G. 1973, *Nature Physical Science*, 246, 93
- Schrijver, C. J. & Pols, O. R. 1993, *A&A*, 278, 515
- Spruit, H. C. 1998, *A&A*, 333, 603
- Spruit, H., & Phinney, E. S. 1998, *Nature*, 393, 139
- Spruit, H. C. 2002, *A&A*, 381, 923
- Tout, C. A., Wickramasinghe, D. T., Liebert, J., Ferrario, L., & Pringle, J. E. 2008, *MNRAS*, 387, 897
- Ventura, P., D’Antona, F., & Mazzitelli, I. 2000, *A&A*, 363, 605
- Vishniac, E. T., & Cho, J. 2001, *ApJ*, 550, 752
- Vishniac, E. T., & Shapovalov, D. 2014, *ApJ*, 780, 144
- Wickramasinghe, D. T., Tout, C. A., & Ferrario, L. 2014, *MNRAS*, 437, 675
- Yakovlev, D. G. & Urpin, V. A. 1980, *Soviet Ast.*, 24, 303
- Zapolsky, H. S. & Salpeter, E. E. 1969, *ApJ*, 158, 809